MASTERARBEIT

Titel der Masterarbeit

„Developmental control of cranial form: global or local?"

verfasst von

Corinna Matiasch BSc

angestrebter akademischer Grad

Master of Science (MSc)

Wien, 2015

Studienkennzahl lt. Studienblatt:	A 066 827
Studienrichtung lt. Studienblatt:	Masterstudium Anthropologie
Betreut von:	Ass.-Prof. Mag. Dr. Philipp Mitteröcker

Contents

1 Abstract

The complexity of cranial anatomy has long been a prominent topic in evolutionary biology. Within the last century a number of studies have focused on morphological integration, canalization and modularity within the cranium. The goal of this thesis is to explore how overall cranial form is achieved in *Homo sapiens* and which mechanisms and regulations are active on which spatial scales, i.e. the overall cranium or the individual bones. Therefore, two models are applied that allow to distinguish between *irregulation/self-similarity*, *coordinated growth* and *compensatory growth* for skull size and shape. 'Irregulation' or 'self-similarity' of development can either occur if the individual parts are under completely independent developmental control, which is of course not compatible with life, or if the positive and negative covariances between the parts, and thus their correlations, cancel each other out. In case of 'coordinated growth', the bones would be positively correlated. In the case of 'compensatory growth', the bones would be negatively correlated.

For analysis, I used three-dimensional CT scans of a geographically and ethnically diverse sample consisting of 30 adult human crania, 14 of them female, 16 male. 65 midsagittal unpaired landmarks were marked on each individual on a visualization of the CT scan in the Amira software package. They were chosen and defined to outline a midsagittal dissection of each cranial bone: frontal, parietal, occipital, temporal, sphenoid, vomer, palatine, maxilla, ethmoid and nasal. The midsagittal plane was defined locally for each landmark. An overall cranial outline, a viscerocranial outline, a neurocranial outline and the individual bones they consist of were defined by corresponding sets of landmarks. The areas for all individual bones and the cranial outlines were calculated from two-dimensional landmarks. Then, the area variances and the area means were calculated for each bone structure and all three outlines and the quotients (area variance divided by area mean) for all structures were determined. Furthermore, the log-transformed variances were regressed on the log-transformed means. To investigate variances in shape, the total variance of the Procrustes coordinates for all bones and the cranial outlines were calculated. Subsequently, the log-transformed shape variances were regressed on the partial warps' log-transformed inverse bending energies.

The overall area variance was clearly larger than the sum of individual area variances in all size calculations. The quotients of the area variances divided by the area means were not the same for all bones. In the regression of the log-transformed area variances on the log-transformed area means the resulting regression slope was > 1. The shape variances for the cranial median sagittal outlines were relatively small in comparison with the contributing bones' shape variances. In the regression of the log-transformed shape variances on the log-transformed inverse bending energy the resulting regression slope was < 1.

These findings indicate that 'coordinated growth' between the bones is the dominating process for

controlling bone size, while 'compensatory growth' is the dominating process for controlling individual bone shape. 'Coordinated growth' regarding size development could be caused by pleiotropic gene expression. The original bone/cartilage condensations in the initial stage of bone formation and patterning should be 'genetically integrated' and the bones' basic size should thus be set by pleiotropic effects from the shared genes. Moreover, this allometric effect could be achieved by pleiotropic genes that cause 'coordinated growth' during ontogeny, growth hormones, etc. 'Compensatory growth' regarding shape development could result from two scenarios of canalization: First, shape could not be directly canalized, but incidentally achieved by epigenetic effects that regulate mechanical strain. Second, shape could be directly canalized and achieved by active correction of the amount of deposited or resorbed bone, which could be controlled via pleiotropy with opposing effects on different bones.

2 Zusammenfassung

Die Komplexität der cranialen Anatomie ist schon lange ein bedeutendes Thema in der Evolutions-
biologie. Innerhalb des letzten Jahrhunderts konzentrierten sich einige Studien auf morphologische
Integration, Kanalisation und Modularität im Cranium. Das Ziel dieser Arbeit ist es zu untersuchen
wie die Gesamtform des Schädels bei *Homo sapiens* zustande kommt und welche Mechanismen und
Regulationen auf welchen räumlichen Skalen (Gesamtschädel oder individuelle Knochen) aktiv sind.
Daher wurden zwei Modelle angewandt, die es erlauben zwischen *irregulation/self-similarity*, *coordi-
nated growth* und *compensatory growth* bei Schädelgröße und -gestalt zu unterscheiden. 'Irregulation'
oder 'self-similarity' der Entwicklung kann entweder vorkommen wenn die einzelnen Teile unter völlig
unabhängiger Entwicklungskontrolle stehen, was natürlich inkompatibel mit dem Leben ist, oder wenn
die positiven und negativen Kovarianzen zwischen den Einzelteilen, und daher deren Korrelationen,
einander aufheben. Im Fall von 'coordinated growth' würden die Knochen positiv korrelieren. Im Fall
von 'compensatory growth' würden die Knochen negativ korrelieren.

Für die Analyse verwendete ich dreidimensionale CT-Scans von 30 geografisch und ethnisch di-
versen menschlichen Crania, 14 davon weiblich, 16 männlich. 65 mediansagittale unpaarige Landmarks
wurden auf jedem Individuum auf einer Visualisierung im Amira Softwarepaket markiert. Sie wur-
den ausgesucht und definiert um einen mediansagittalen Schnitt jedes Schädelknochens zu umranden:
Os frontale, Os parietale, Os occipitale, Os temporale, Sphenoid, Vomer, Os palatinum, Maxilla, Os
ethmoidale und Os nasale. Die medialsagittale Ebene wurde lokal für jedes Landmark definiert. Eine
Gesamtschädel-Outline, eine viscerocraniale Outline, eine neurocraniale Outline und die individu-
ellen Knochen aus denen diese bestehen wurden durch korrespondierende Landmarks definiert. Die
Flächen aller individuellen Knochen und Schädeloutlines wurden mit zweidimensionalen Landmarks
berechnet. Dann wurden die Flächenvarianzen und -mittelwerte aller Knochen und Outlines berech-
net, sowie deren Quotienten (Flächenvarianz dividiert durch Flächenmittelwert). Desweiteren wurde
eine Regression der logarithmierten Varianzen auf die logarithmierten Mittelwerte durchgeführt. Um
die Gestaltvarianzen zu untersuchen, wurden die totalen Varianzen der Procrusteskoordinaten aller
Knochen und Schädeloutlines berechnet. In Folge wurde eine Regression der logarithmierten Gestalt-
varianzen auf die logarithmierten inversen Bending Engeries der Partial Warps durchgeführt.

Die Flächenvarianz der Outline war deutlich größer als die Summe der Varianzen der einzel-
nen Flächen in allen Größenberechnungen. Die Quotienten der Flächenvarianzen dividiert durch
die Flächenmittelwerte waren nicht gleich für alle Knochen. In der Regression der logarithmierten
Flächenvarianzen auf die logarithmierten Flächenmittelwerte war die berechnete Steigung > 1. Die
Gestaltvarianzen der cranialen mediansagittalen Outlines waren relativ klein im Vergleich zu den
Gestaltvarianzen der beitragenden Knochen. In der Regression der logarithmierten Gestaltvarianzen

auf die logarithmierten inversen Bending Energies war die berechnete Steigung < 1.

Diese Resultate weisen darauf hin, dass 'coordinated growth' zwischen den Knochen der dominante Prozess für Größenkontrolle ist, während 'compensatory growth' der dominante Prozess für Gestaltkontrolle ist. 'Coordinated growth' in der Größenentwicklung könnte durch pleiotropische Genexpression verursacht werden. Die ursprünglichen Knochen/Knorpel-Kondensationen im anfänglichen Stadium der Knochenformation und -anordnung sollten 'genetisch integriert' sein und die grundlegende Größe der Knochen sollte daher durch pleiotropische Effekte der geteilten Gene festgelegt werden. Desweiteren könnte dieser allometrische Effekt durch pleiotropische Gene, die 'coordinated growth' im Laufe der ontogenetischen Entwicklung verursachen, Wachstumshormone, etc. zustande kommen. 'Compensatory growth' in der Gestaltentwicklung könnte durch zwei Szenarios von Kanalisation entstehen: Erstens, könnte Gestalt nicht direkt kanalisert sein, sondern zufällig zustande kommen durch epigenetische Effekte, die den mechanischen Druck regulieren. Zweitens, könnte die Gestalt direkt kanalisert sein und durch aktive Korrektur der Menge an abgelagertem und resorbiertem Knochen erreicht werden, die durch Pleiotropie mit entgegengesetzten Effekten auf unterschiedliche Knochen kontrolliert werden könnte.

3 Introduction

The complexity of cranial anatomy has long been a prominent topic in evolutionary biology. The phylogenetic origins and ontogenetic development of its individual bones has been thoroughly researched. Within the last century, the cranium has been a particular focus of research conducted under the keyword *morphological integration*. The term was coined by Olson and Miller in 1958 and is similar to the concept of 'correlation pleiades' (Terentjev 1931; Berg 1960). The basic idea behind 'morphological integration' is that morphological traits are correlated and covary, if they are influenced by common factors. On the individual level, these factors are mainly functional and/or developmental. In other words, traits which are functionally or developmentally linked will covary in a population. Those traits are then referred to as integrated traits.

Hallgrímsson et al. (2009) proposed a different definition of 'integration', focusing not on actual observed covariation, since a prerequisite for covariation is variation within a population, but on the capacity of traits to covary. As an analogy for their definition, Hallgrímsson et al. (2009) gave Wagner et al.'s (1997) dispositional definiton of variability: "Variation can be directly observed as a property of a collection of items. In contrast, variability is a term that describes the potential or the propensity to vary. Variability is thus the ability to vary." Thus, Hallgrímsson et al. (2009) suggested that *covariability* may be a more suitable term to describe 'integration'.

An extensive number of studies endeavored to assess cranial 'integration', especially with regard to development and phylogeny (e.g. Ackermann 2002; Cheverud 1982; Lieberman et al. 2002; Mitteroecker and Bookstein 2008; Drake and Klingenberg 2010; Goswami 2006; Hallgrimsson et al. 2007; Marroig et al. 2009; Zelditch and Carmichael 1989; Porto et al. 2009; Roseman et al. 2011; Singh et al. 2012). It has been proposed, however, that many studies neglect the manifold nature of sources of covariance in their interpretation of results (Mitteroecker et al. 2012). For example, the correlated nature of measurements themselves (e.g. due to local proximity or shared landmarks) as a source of covariance is often disregarded. Biological sources of covariation between traits are *genetic* and *environmental integration*, as distinguished by Cheverud (1982; 1996; 1996). In the former case, the association between morphological components is due to genetic influences such as pleiotropy or linkage disequilibrium. In the latter, 'integration' during development is affected in a non-heritable way. Ideally, conclusions should not be drawn from mere "interpretation of raw covariances" (Mitteroecker et al. 2012).

A concept closely related to 'morphological integration' is *modularity* or *variational modularity*. Müller (2007) explained that modules in biological organization are characterized "by their greater internal (intramodule) than external (intermodule) integration, by their repetitiveness and by their evolutionary persistence and reuse". Mitteroecker (2009) wrote that "modules often are defined as

organismal parts with local and independent (dissociated) genetic and developmental control". Such genetically and developmentally uncorrelated modules should result in functionally uncorrelated traits. These should be separately influenced by selection. Thus, *evolvability*, "the ability of a population to evolve in the direction of selection when stabilizing selection is absent" (Wagner and Altenberg 1996; Hansen and Houle 2008), should be higher for functional modules that are controlled by genetic and developmental modules and influences their response to selection (Mitteroecker et al. 2012). It follows that traits which are functionally correlated should also be genetically correlated to facilitate joint evolution and to increase their evolvability (Mitteroecker et al. 2012). However, phenotypic variation that is described as 'modular' due to its modular covariance structure can, on a microevolutionary scale, i.e. for traits with small phenotypic and genetic variation, also be explained by overlapping sets of pleiotropic factors (Mitteroecker 2009). Moreover, Pavlicev and Hansen (2011) and Hansen (2003) have demonstrated that overlapping pleiotropic factors increase genetic variance and thereby promote evolvability more than 'modular' genotype-phenotype maps. Nonetheless, as the relationship between genetic and developmental factors and phenotypic traits is non-linear over a larger range of variation, i.e. on a macroevlutionary scale, the pleiotropic effects and a population's covariance structure are sensitive to changes in the phenotypic mean (Mitteroecker 2009; Mitteroecker et al. 2012). Thus, Mitteroecker (2009) and Pavlicev and Hansen (2011) have found that with regard to more comprehensive evolutionary changes genotype-phenotype maps following a 'modular' organization and constrained pleiotropic effects are more consequential for increasing evolvability. Mitteroecker (2009) concluded that an overlapping and hierarchical combination of local and pleiotropic effects is most likely to explain the development of organisms.

Another way to examine functionally linked traits is regarding it under the keyword *canalization*. 'Canalization' was originally defined by Waddington (1942) as "[a]djustment of developmental reactions so as to bring about one definite end result regardless of minor variations in conditions during the course of the reaction". A related term, 'autoregulatory mechanism', was introduced by Schmalhausen (1949) as a group of processes that regulate a developmental path against environmental and genetic influences. More recent definitions of 'canalization' were provided by Stearns et al. (1995), a "process by which phenotypic variation is reduced by developmental mechanisms", and by Wagner et al. (1997), "[t]he suppression of phenotypic variation". Since functionally linked traits, such as overall cranial composition, can only maintain proper function if variation in their morphological outcome is constrained, it seems that the overall structure of functionally linked traits should be restricted in variability, in other words the traits should be 'canalized' in the dysfunctional directions.

Zelditch et al. (2006) suggested that 'canalization' shapes patterns of 'integration' in mammalian skulls. They hypothesized that skull shape is 'monitored' and that a "constancy of variation results

from a balance between processes that generate and remove variation"; thereby "variation is continually generated but fails to accumulate because it is equally rapidly removed". They suggested that coordinated growth caused by genetic pleiotropy does not explain the stability of variation in skull shape, whereas compensatory differential growth does.

The goal of this thesis is to explore how overall cranial form is achieved in *Homo sapiens* and which mechanisms and regulations are active on which spatial scales. Therefore, let us first consider a toy model, devised by my supervisor, of a structure that consists of two parts, so that the area S of the entire structure is the sum of the areas A and B:

$$S = A + B.$$

Hence, the average areas also add up:

$$\mathrm{E}(S) = \mathrm{E}(A) + \mathrm{E}(B).$$

The variance of the whole structure $\mathrm{Var}(S) = \mathrm{Var}(A + B)$ can be broken down into the variances of the components A and B plus twice their covariance:

$$\mathrm{Var}(A + B) = \mathrm{Var}(A) + \mathrm{Var}(B) + 2\mathrm{Cov}(A, B).$$

Three different cases can be distinguished in this toy model:

(i) The parts A and B are uncorrelated. The covariance between A and B is 0 and therefore the variance of the whole equals the sum of the variances of the parts:

$$\mathrm{Var}(A + B) = \mathrm{Var}(A) + \mathrm{Var}(B).$$

This scenario can occur if the individual parts are under completely independent developmental control. We will refer to this case as *irregulation*, characterized by the absence of regulation and, therefore, correlation between the parts.

(ii) The parts A and B are positively correlated. The covariance between A and B is larger than 0. As a result, the whole structure's variance is larger than the summed variances of its parts:

$$\mathrm{Var}(A + B) > \mathrm{Var}(A) + \mathrm{Var}(B).$$

This scenario can occur if parts need to correspond in size in order to function, for example when allometric size variation plays a role in the structure. We will refer to this case as *coordinated growth*, characterized by positive correlation between the individual parts and an overall structure that is more variable than its parts. This scenario strongly resembles the typical notion of 'integration'.

(iii) The parts A and B are negatively correlated. The covariance between A and B is smaller than 0 and therefore the variance of the whole is smaller than the sum of the variances of its parts:

$$\text{Var}(A + B) < \text{Var}(A) + \text{Var}(B).$$

This scenario can occur if compensation between the parts plays a role in the structure. We will refer to this case as *compensatory growth*, characterized by negative correlation between the individual parts and an overall structure that is less variable than its parts.

If we extend this toy model to a structure with more than two parts, so that the area S of the entire structure is the sum of the areas of its parts: $S = A + B + C + D$, then the variance of the whole structure can be broken down into the sum of the variances of the components plus twice all their pairwise covariances:

$$\text{Var}(A + B + C + D) =$$

$$\text{Var}(A) + \text{Var}(B) + \text{Var}(C) + \text{Var}(D) + 2\text{Cov}(A,B) + 2\text{Cov}(A,C) + 2\text{Cov}(A,D) + 2\text{Cov}(B,C)$$

$$+2\text{Cov}(B,D) + 2\text{Cov}(C,D).$$

Here we can see more clearly that 'irregulation' of development, can either occur if the individual parts are under completely independent developmental control, which is of course not compatible with life, or if the positive and negative covariances between the parts, and thus their correlations, cancel each other out. In other words, the mean of all covariances would be 0. If the mean covariance is positive, 'coordinated growth' is dominant and if the mean covariance is negative 'compensatory growth' is dominantly operative.

To come back to the aim of this thesis, exploring how overall cranial form is achieved in *Homo sapiens*, let us assume that the area of a midsagittal section through the human skull is analogous to area S. Then the areas of midsagittal sections through the individual bones are analogous to the parts that add up to S. In accordance with our toy model, the variance of overall cranial area is the sum of the variances of all individual bone areas plus twice their pairwise covariances.

If the individual bones were uncorrelated or their positive and negative covariances canceled each other out, this would result in a net covariance of 0 between them, meaning the variance of overall cranial area equals the sum of the individual bone areas' variances. This would be a case of 'irregulation' where either the individual bones are under completely independent local control, which is highly unlikely, or the individually positive and negative correlations between the bones cancel each other out.

If cranial developmental control was on overall form, however, there could either be 'coordinated' or 'compensatory growth' dominating between the separate bones. In case of 'coordinated growth',

the bones would be positively correlated, i.e. we would find a positive net covariance between them and overall cranial form would be more variable than the sum of its parts. This can result, for example, from allometry between the bones. In the case of 'compensatory growth', the bones would be negatively correlated, i.e. we would find a negative net covariance between them and the individual bones would in sum be more variable than the overall cranial structure.

Following from these scenarios, a comparison of the variances in size and shape of individual bones and the overall cranial form should demonstrate on which of them and how developmental control acts to achieve overall form. As it is also conceivable that different control options are active, but restricted to specific regions of the cranium, the same hypothesis can be tested on different subunits of the cranium: the neurocranium and the viscerocranium.

Since the shapes of the individual bones do not add up to the overall shape, a different approach has to be considered to make further analyses regarding shape. Bookstein (2015) recently suggested that one of the standard tools for analyzing 'morphological integration', the Procrustes distribution, is flawed by the same principle as many other studies on the topic (see above): the Procrustes analysis treats landmarks as if they were statistically independent of each other and of their mean. As a solution, he proposed a procedure analogous to the treatment of trend in time series in paleobiology. In this procedure the landmark data's prinicipal warp scores are mathematically manipulated to make the data *self-similar*, meaning its distribution is the same for every scale. If the log-transformed variances of the principal warp scores are graphed against their log-transformed specific bending energies, the resulting regression slope is -1. The regression slope of the non-manipulated data (again the principal warp scores' log-transformed variances graphed against their log-transformed specific bending energies) can now be compared to the 'self-similar' null-model; depending on whether the slope falls off faster or more slowly, the data set can be interpreted as 'integrated' or 'disintegrated', respectively, which Bookstein (2015) defined as "two modes of organismal variation according to which morphometric data can deviate from this common null [i.e. 'self-similarity'], which, as in the temporal domain, is formally featureless, incapable of supporting any summary beyond a single parameter for amplitude". It is important to remember now that if the shape of a structure is 'self-similar', its distribution is the same for every scale and its log-transformed shape variances and log-transformed specific bending energies scale linearly with each other and will produce a regression slope of -1.

Let us now consider size and go back to our toy model of 'irregulation'. We know that if the areas A and B add up to area S:

$$S = A + B,$$

the average areas also add up:

$$\mathrm{E}(S) = \mathrm{E}(A) + \mathrm{E}(B).$$

In an instance of 'irregulation' between the individual parts, the individual area variances add up to the variance of the entire structure:

$$\mathrm{Var}(A + B) = \mathrm{Var}(A) + \mathrm{Var}(B).$$

Hence, we can see that in an 'irregulated' structure the average of the area scales linearly with the variance of the area. The variance of area A divided by the mean of area A would yield the same result as the variance of area B divided by the mean of area B:

$$\frac{\mathrm{Var}(A)}{\mathrm{E}(A)} = \frac{\mathrm{Var}(B)}{\mathrm{E}(B)}.$$

Thus, we see that differently sized parts show the same variational properties relative to their scale: the structure is 'self-similar' in its variational properties across different spatial scales. Furthermore, when regressing the log-transformed variances on the log-transformed means, the resulting regression slope is 1. It is now clear that 'irregulation' of size is analogous to 'self-similarity' of shape.

To make the interpretations of both more easily comparable, the log-transformed shape variances can be regressed on the log-transformed *inverse* specific bending energies, as bending energy inversely relates to scale. The resulting regression slope will then be 1 in case of 'self-similarity', just as the regression slope for 'irregulation'.

Bookstein (2015) interpreted a slope of < -1 as an indication for 'integration' of shape, while a slope of > -1 indicates 'disintintegration'. With the proposed change to inverse bending energy, the interpretation would instead be 'integration' for a slope > 1 and 'disintegration' for a slope < 1. For size, a slope of > 1 can be interpreted as an indication for 'coordinated growth', while a slope of < 1 can be interpreted as an indication for 'compensatory growth'.

Since Bookstein (2015) is still negotiating the terminology for the outcomes 'integration' and 'disintegration', a case could be made to extend the terms 'coordinated growth' and 'compensatory growth' to the analysis of shape. For size as well as for shape, 'coordinated growth' could be interpreted as integrated growth where the individual parts are positively correlated, while 'compensatory growth' could be interpreted as integrated growth where the individual parts are negatively correlated. The results for the state that Bookstein (2015) has so far been calling 'disintegration' could perhaps better be explained by 'integration' where the individual (in this case undefined) modules display 'compensatory growth'. 'Self-similarity' and 'irregulation', therefore, seem to refer to the same state: positive and negative correlations between the parts cancel each other. The mathematical relationships, however, have yet to be worked out.

Within this thesis I hope to find insights into the mechanisms operating to achieve the cranial form of *Homo sapiens*: Are shape and size of individual bones or the cranium constantly 'monitored' and regulated, as Zelditch et al. (2006) suggested could be implied for 'compensatory growth'? How would

the necessary signals be created and transmitted? What could be the nature of the used signals? For example, could the mechanical loads the bones put on each other by physically interacting be a signal? Or do the mechanical loads applied onto the bones by brain, muscles or other soft tissues play a role in regulation? Could epigenetic processes triggered by these interactions influence gene expression (Zelditch et al. 2004)? – These are some of the questions I will explore.

4 Material and methods

4.1 Specimens

I used three-dimensional CT scans of a geographically and ethnically diverse sample consisting of 30 adult human crania, 14 of them female, 16 male. 19 crania were Europeans, the remaining crania were Africans and Australians. Details on the specimens can be seen in Tab. 1.

4.2 Landmarks and preprocessing

The 30 CT scans were visualized in the Amira software package (v5.6). On each individual, 65 midsagittal unpaired landmarks (Fig. 1), 19 of which are anatomical landmarks (Tab. 2), were marked using isosurfaces, volume renderings (Fig. 2, 3) and the CT slices for orientation within the data. They were chosen and defined to outline a midsagittal dissection of each cranial bone: frontal, parietal, occipital, temporal, sphenoid, vomer, palatine, maxilla, ethmoid and nasal. Because the skull is not perfectly symmetric, the midsagittal plane was defined locally for each landmark.

The landmark data were then imported into Mathematica (v10.1.0.0), where the three-dimensional coordinates were converted into two-dimensional ones by projecting the landmarks onto a plane spanned by the axes of each individual's first two principal components. The local definition of the midsagittal plane in the original data set made this conversion step necessary to derive one midsagittal plane for all landmarks.

The next step was to define the semilandmarks and curves on which these semilandmarks could slide. Semilandmarks, by definition, "are points on smooth curves, for which the exact location on the curve cannot be identified and hence is statistically estimated" (Mitteroecker et al. 2013). These curves are approximated by tangents, taken as vectors through both neighboring landmarks of each semilandmark, translated until they cross the semilandmark. The semilandmarks are then slid on their curves using the sliding landmark algorithm, which minimizes the bending energy between the landmark configuration and the sample average (Bookstein 1997; Gunz et al. 2005; Gunz and Mitteroecker 2013). The resulting semilandmark configuration is geometrically homologous for all specimens across the sample (Fig. 4).

Then an overall cranial outline, a viscerocranial outline, a neurocranial outline and the individual bones they consist of were defined by corresponding sets of landmarks (Tab. 3, 4, 5, 6, 7 and 8). These three types of cranial outline were defined to account for the functional and structural differences between viscerocranium and neurocranium. The bones were defined differently for the size and shape analyses, since the size calculations required that no bone dissection consisted solely of a line, while lines could effortlessly be handled in the shape calculations. Visualizations of bones for size and shape

analyses were constructed for all individuals (Fig. 5, 6, 7, 8, 9 and 10). As the suture between the sphenoid and the occipital normally fuses at an age of 18 to 25 years (White and Folkens 2005), its position had to be estimated. To minimize resulting error, two alternatives were defined for each bone: one separates the bones approximately where the sphenooccipital suture would have been, the other takes the foramen magnum as the separating structure. Alternative definitions of the ethmoid and sphenoid were used to assess the influence of single landmarks. (For details on the bone alternatives see p. 50).

Next, a Generalized Procrustes Analysis was separately performed on the coordinates of each individual bone, the overall cranial outline, the viscerocranial outline and the neurocranial outline to obtain shape variables for the 30 individuals. In the Procrustes Analysis the square root of the average squared distance was used as centroid size to account for the different number of landmarks. Shape variables comprise the geometric properties of an object, in this case the bone, that are invariant to translation, rotation and scaling. In contrast, form variables include information on shape and size, and thereby are invariant only to translation and rotation. Both kinds of variables are needed for the following analyses.

The standard three-step procedure for a Procrustes superimposition of two objects is least-squares based (Bookstein 1997; Dryden and Mardia 1998). First, the objects are centered by translating their centroids (the average of their coordinates) above each other. Second, the objects are scaled to the same centroid size, which is the square root of the summed squared distances between the coordinates and their centroid. Third, one object is rotated around its centroid until the sum of the squared distances between all homologous landmarks of the two objects are at a minimum. For analyses of more than two objects, this standard procedure has been extended to the Generalized Procrustes Analysis (GPA), where the rotation process in the third step is extended to an iterative algorithm (Gower 1975; Rohlf and Slice 1990). The resulting landmark coordinates are called Procrustes shape coordinates and include information only on the shape of their objects.

A principal component analysis (PCA) of the Procrustes data was carried out and the first six eigenvectors were extrapolated and visualized using polygons. The PCA was furthermore used to look for outliers in the data set and thereby to check against measurement errors. For the same purpose, a landmark vector plot was used to compare differences between individuals.

4.3   Analysis of size

The areas for all individual bones and the cranial outlines were calculated from the two-dimensional landmarks. Then, the area variances and the area means were calculated for each bone structure and all three outlines and their quotients (area variance divided by area mean) for all structures were

determined. Furthermore, the log-transformed variances were regressed on the log-transformed means.

4.4   Analysis of shape

To investigate variances in shape, the total variance of the Procrustes coordinates for all bones and the cranial outlines were calculated and divided by the respective number of landmarks per structure to make variance independent of the number of landmarks. Subsequently, the log-transformed shape variances were regressed on the partial warps' log-transformed inverse bending energies.
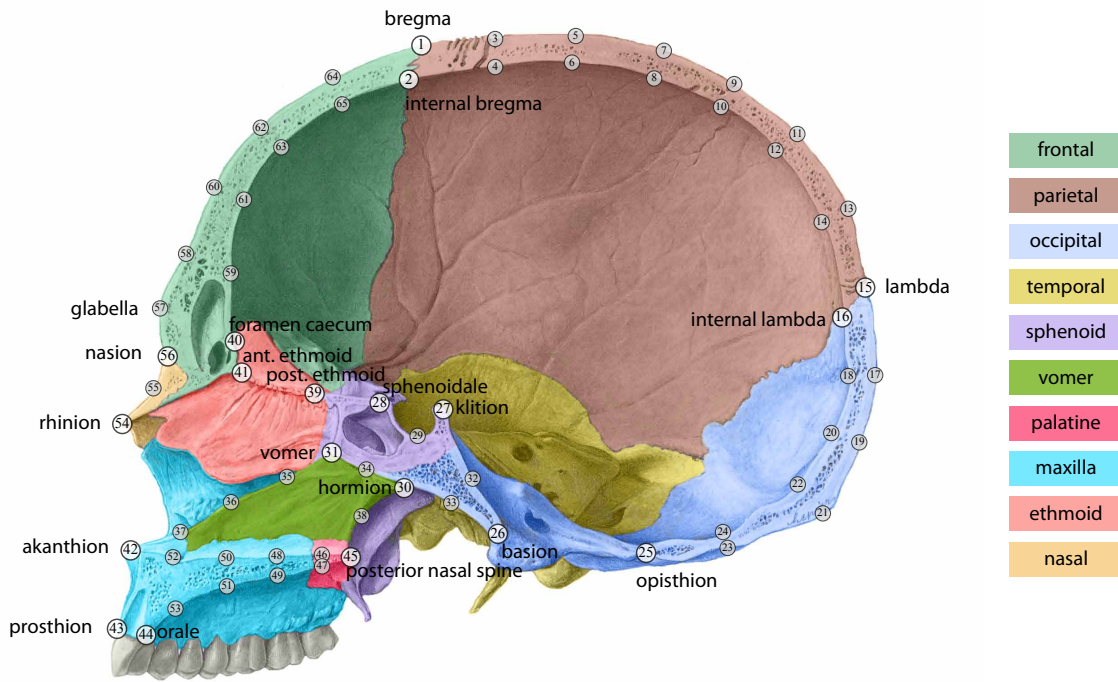
Figure 1: Midsagittal view of a human cranium showing 19 landmarks and 46 semilandmarks. Semilandmarks are shown in smaller grey circles. [Adapted from Putz and Pabst 2008.]

Table 1: Sex, age, origin and CT resolution for used specimens.

No.	Specimen	Sex	Age	Origin	CT Resolution (x, y, z in mm)
1	VA-001	female	adult	Europe	$0.426 \times 0.426 \times 1.000$
2	VA-002	male	mature	Europe	$0.426 \times 0.426 \times 1.000$
3	VA-003	male	adult	Europe	$0.467 \times 0.467 \times 1.000$
4	VA-004	female	adult	Europe	$0.377 \times 0.377 \times 1.000$
5	VA-007	male	adult	Europe	$0.426 \times 0.426 \times 1.000$
6	VA-012	male	mature	Europe	$0.445 \times 0.445 \times 1.000$
7	VA-013	female	adult	Australia	$0.426 \times 0.426 \times 1.000$
8	VA-014	female	adult	Africa	$0.467 \times 0.467 \times 1.000$
9	VA-017	male	adult	Australia	$0.467 \times 0.467 \times 1.000$
10	VA-019	female	adult	Africa	$0.467 \times 0.467 \times 1.000$
11	VA-020	male	mature	Australia	$0.516 \times 0.516 \times 1.000$
12	VA-021	male	mature	Europe	$0.445 \times 0.445 \times 1.000$
13	VA-022	male	mature	Europe	$0.467 \times 0.467 \times 1.000$
14	VA-024	female	adult	Africa	$0.490 \times 0.490 \times 1.000$
15	VA-025	male	adult	Africa	$0.516 \times 0.516 \times 1.000$
16	VA-030	female	adult	Europe	$0.426 \times 0.426 \times 1.000$
17	VA-050	female	adult	Europe	$0.449 \times 0.449 \times 1.000$
18	VA-051	female	adult	Australia	$0.396 \times 0.396 \times 0.400$
19	VA-052	male	mature	Australia	$0.408 \times 0.408 \times 0.400$
20	VA-053	female	adult	Africa	$0.296 \times 0.296 \times 1.000$
21	ULAC-012	male	adult	Europe	$0.388992 \times 0.388992 \times 0.388993$
22	ULAC-013	female	adult	Europe	$0.332067 \times 0.332067 \times 0.332066$
23	ULAC-016	male	adult	Europe	$0.332556 \times 0.33256 \times 0.332559$
24	ULAC-019	male	adult	Europe	$0.389481 \times 0.389481 \times 0.389483$
25	ULAC-033	male	adult	Europe	$0.332556 \times 0.332556 \times 0.332554$
26	ULAC-039	female	adult	Europe	$0.332571 \times 0.332571 \times 0.332572$
27	ULAC-058	male	adult	Europe	$0.332489 \times 0.332489 \times 0.33249$
28	ULAC-066	female	adult	Europe	$0.2137 \times 0.2137 \times 0.2137$
29	ULAC-210	male	adult	Europe	$0.2137 \times 0.2137 \times 0.2137$
30	ULAC-316	female	adult	Africa	$0.21368 \times 0.21368 \times 0.21368$

Table 2: Landmark definitions (White and Folkens 1991; Martin and Saller 1957). No. 57 was treated as a semilandmark in the analysis.

No.	Landmark	Definition
1	bregma	the intersection point of the coronal and sagittal sutures
2	internal bregma	the point orthogonal to bregma on the lamina interna of the braincase
15	lambda	the intersection point of the sagittal and lambdoidal sutures
16	internal lambda	the point orthogonal to lambda on the lamina interna of the braincase
25	opisthion	the intersection point of the posterior margin of the foramen magnum and the the midsagittal plane
26	basion	the intersection point of the anterior margin of the foramen magnum and the the midsagittal plane
27	klition	the intersection point of the top of the dorsum sellae and the midsagittal plane
28	sphenoidale	the intersection point of the sulcus chiasmatis and the midsagittal plane anterior of the tuberculum sellae
30	hormion	the most posterior midsagittal point of the vomer
31	vomer	the uppermost point of separation between the vomer and the sphenoid bone
39	'posterior ethmoid'	the point of separation between the ethmoid and the sphenoid bone at the base of the crista galli
40	'foramen caecum'	the superior point of separation between the ethmoid and the frontal bone
41	'anterior ethmoid'	the inferior point of separation between the ethmoid and the frontal bone
42	akanthion	the topmost point of the spina nasalis anterior
43	prosthion	the most anterior midsagittal point on the alveolar ridge
44	orale	the orthogonal projection of prosthion onto the interior alveolar ridge between the central incisors
45	'posterior nasal spine'	the most posterior point of the spina nasalis
54	rhinion	the most anterior point of the internasal suture
56	nasion	the highest midsagittal point of the nasal bone
57	glabella	the most anterior midsagittal point of the frontal bone
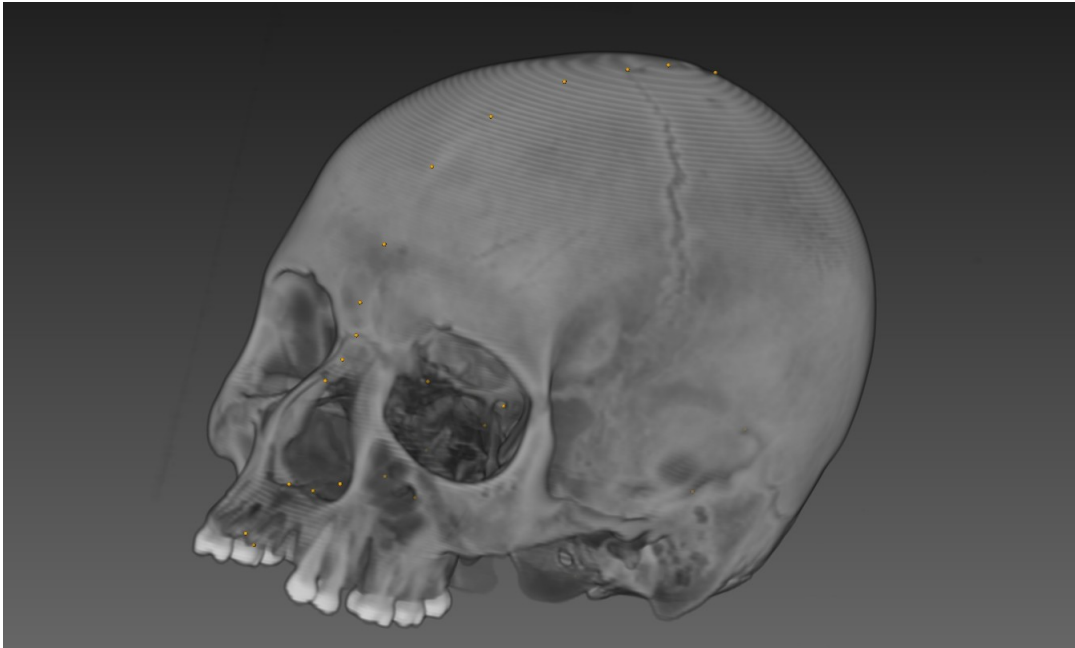
Figure 2: Volume rendering generated from a CT scan of a human cranium.
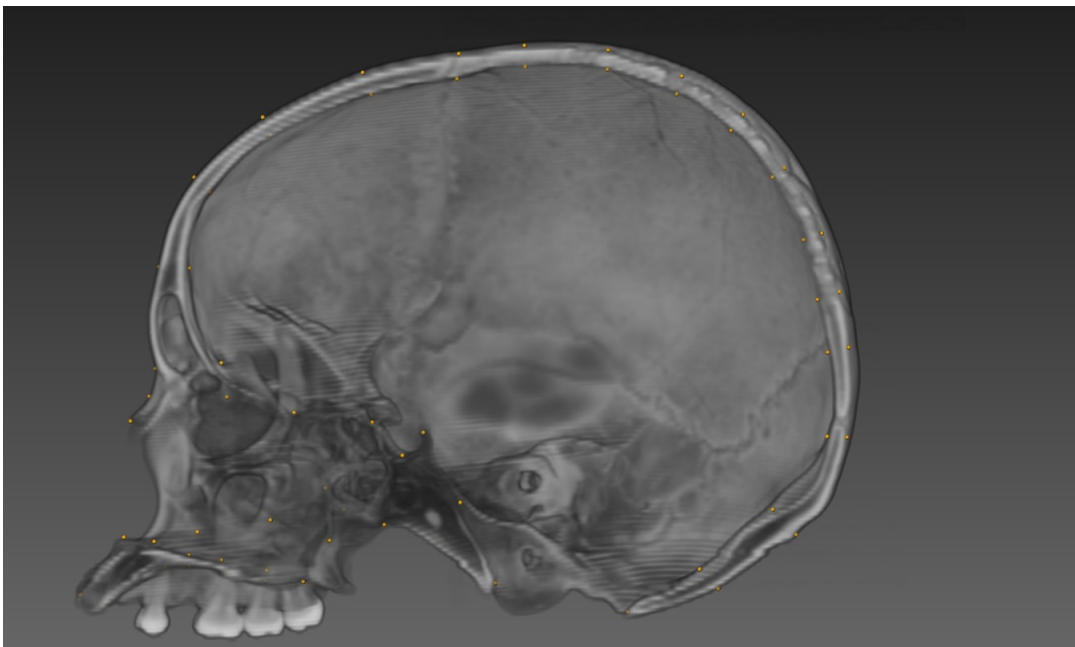
Figure 3: Midsagittal view of a volume rendering generated from a CT scan of a human cranium and landmarks created in Amira.
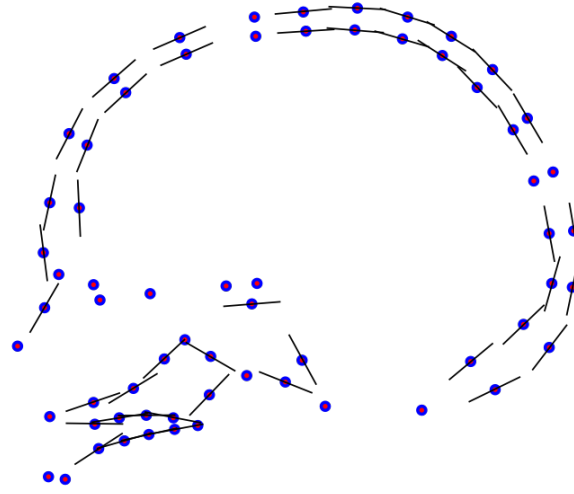
Figure 4: Sliding midsagittal semilandmarks and their associated tangents.

Table 3: Landmark assignments for size analysis of the overall cranium.

structure	assigned landmarks
outline	54, 55, 56, 57, 58, 60, 62, 64, 1, 3, 5, 7, 9, 11, 13, 15, 17, 19, 21, 23, 25, 26, 33, 30, 38, 45, 47, 49, 51, 53, 44, 43, 42
frontal	1, 64, 62, 60, 58, 57, 56, 41, 40, 59, 61, 63, 65, 2
parietal	1, 3, 5, 7, 9, 11, 13, 15, 16, 14, 12, 10, 8, 6, 4, 2
occipitalpart	15, 17, 19, 21, 23, 25, 24, 22, 20, 18, 16
clivus	26, 32, 27, 30, 33
sphenoid	27, 29, 28, 39, 31, 34, 30
vomer	31, 35, 36, 37, 42, 52, 50, 48, 46, 45, 38, 30, 34
maxilla	42, 43, 44, 53, 51, 49, 47, 45, 46, 48, 50, 52
nasal cavity	54, 41, 39, 31, 35, 36, 37, 42
pseudonasal	54, 55, 56, 41
braincase	41, 40, 59, 61, 63, 65, 2, 4, 6, 8, 10, 12, 14, 16, 18, 20, 22, 24, 25, 26, 32, 27, 29, 28, 39
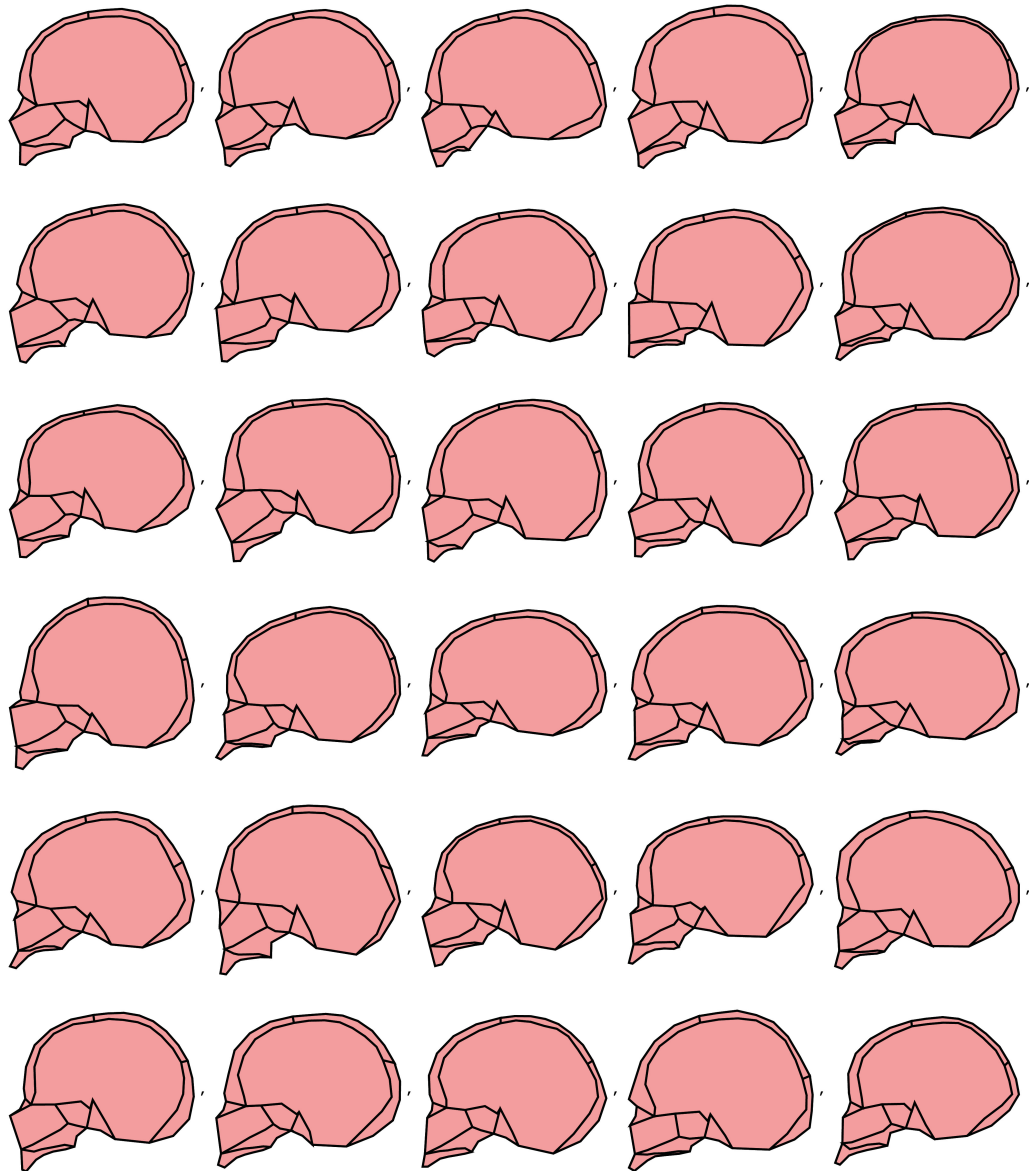
Figure 5: All individuals visualized as polygons for size analysis.

Table 4: Landmark assignments for size analysis of the viscerocranium.

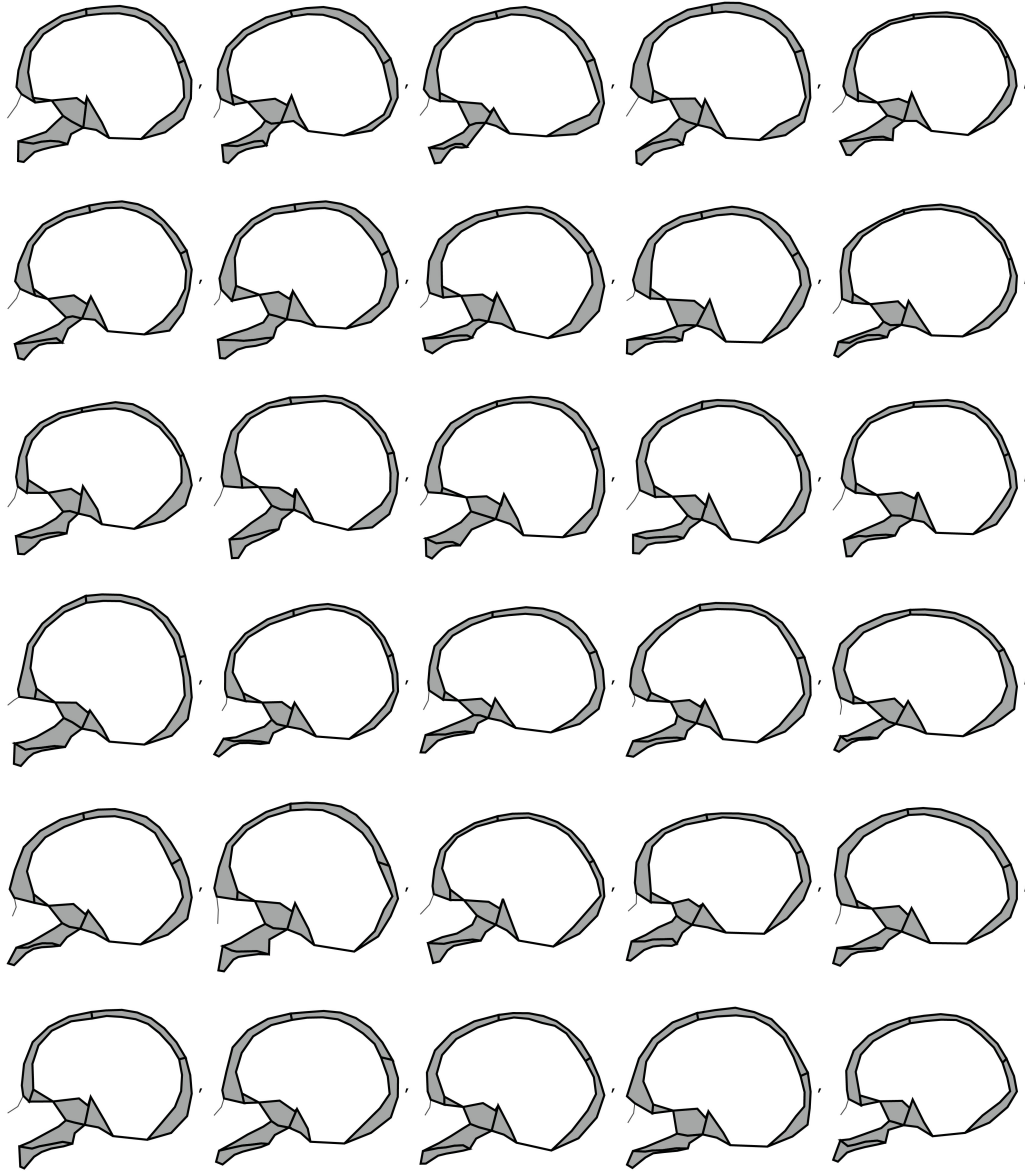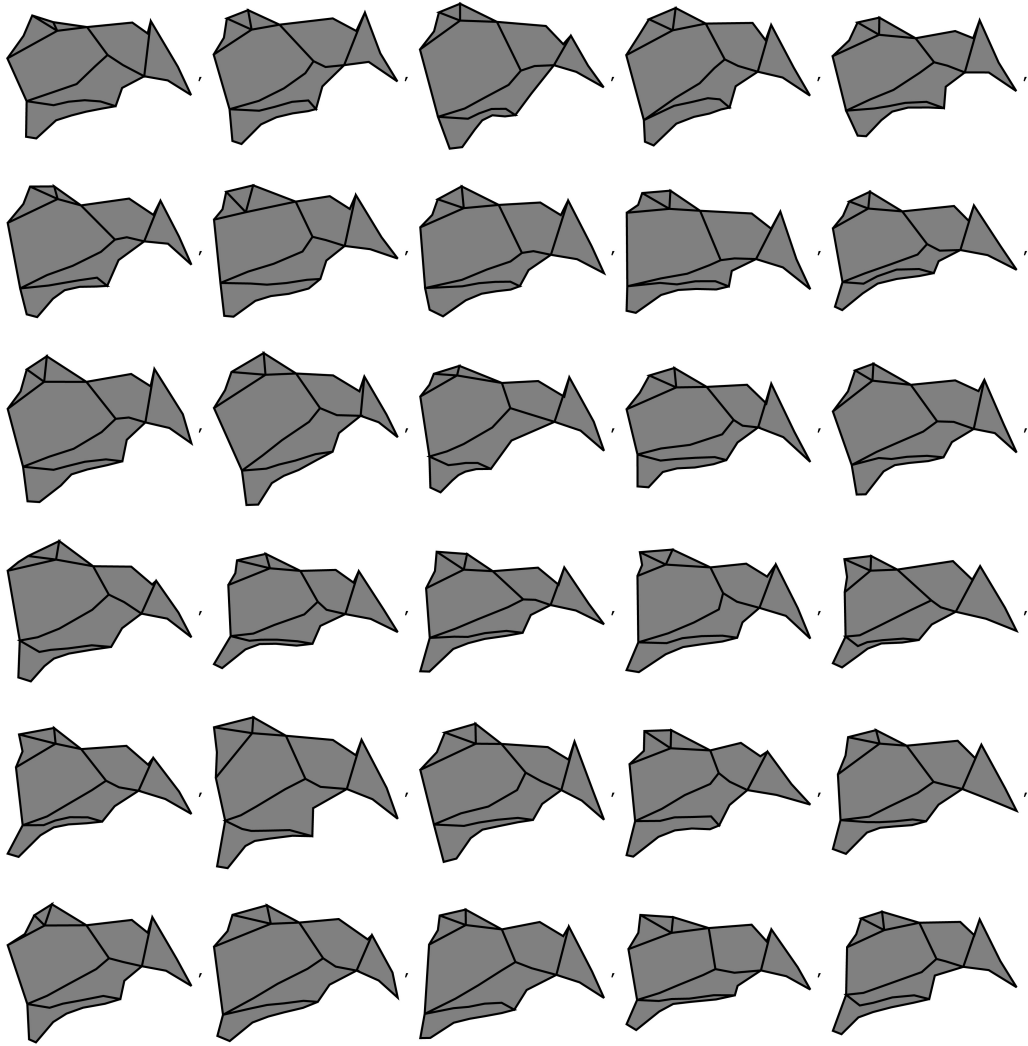| structure	assigned landmarks
viscerocranial outline	56, 55, 54, 42, 43, 44, 53, 51, 49, 47, 45, 38, 30, 33, 26, 32, 27, 29, 28, 39, 41
clivus	26, 32, 27, 30, 33
sphenoid	27, 29, 28, 39, 31, 34, 30
vomer	31, 35, 36, 37, 42, 52, 50, 48, 46, 45, 38, 30, 34
maxilla	42, 43, 44, 53, 51, 49, 47, 45, 46, 48, 50, 52
nasal cavity	54, 41, 39, 31, 35, 36, 37, 42
pseudonasal	54, 55, 56, 41
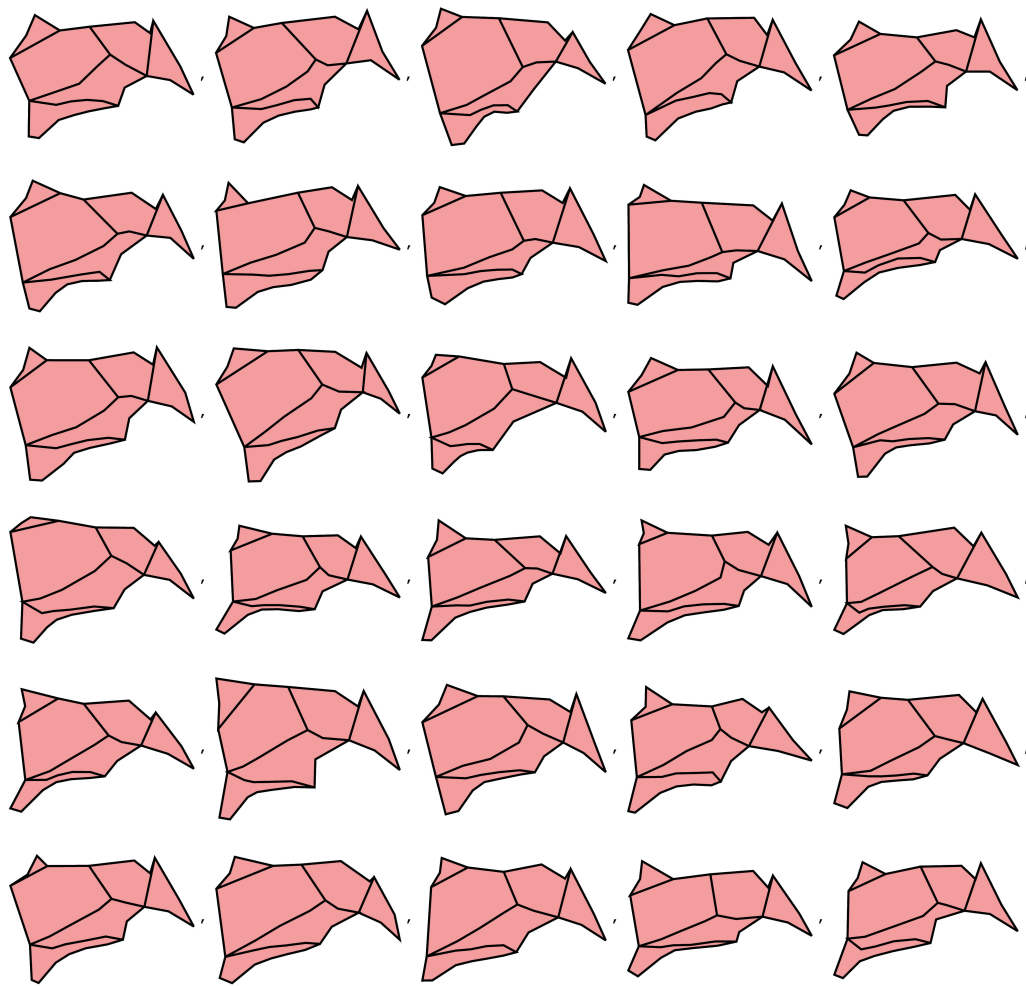
Figure 6: All individuals' viscerocrania visualized as polygons for size analysis.

Table 5: Landmark assignments for size analysis of the neurocranium.

| structure	assigned landmarks
neurocranial outline	56, 57, 58, 60, 62, 64, 1, 3, 5, 7, 9, 11, 13, 15, 17, 19, 21, 23, 25, 26, 33, 30, 34, 31, 39, 41
frontal	1, 64, 62, 60, 58, 57, 56, 41, 40, 59, 61, 63, 65, 2
parietal	1, 3, 5, 7, 9, 11, 13, 15, 16, 14, 12, 10, 8, 6, 4, 2
occipitalpart	15, 17, 19, 21, 23, 25, 24, 22, 20, 18, 16
clivus	26, 32, 27, 30, 33
sphenoid	27, 29, 28, 39, 31, 34, 30
braincase	41, 40, 59, 61, 63, 65, 2, 4, 6, 8, 10, 12, 14, 16, 18, 20, 22, 24, 25, 26, 32, 27, 29, 28, 39
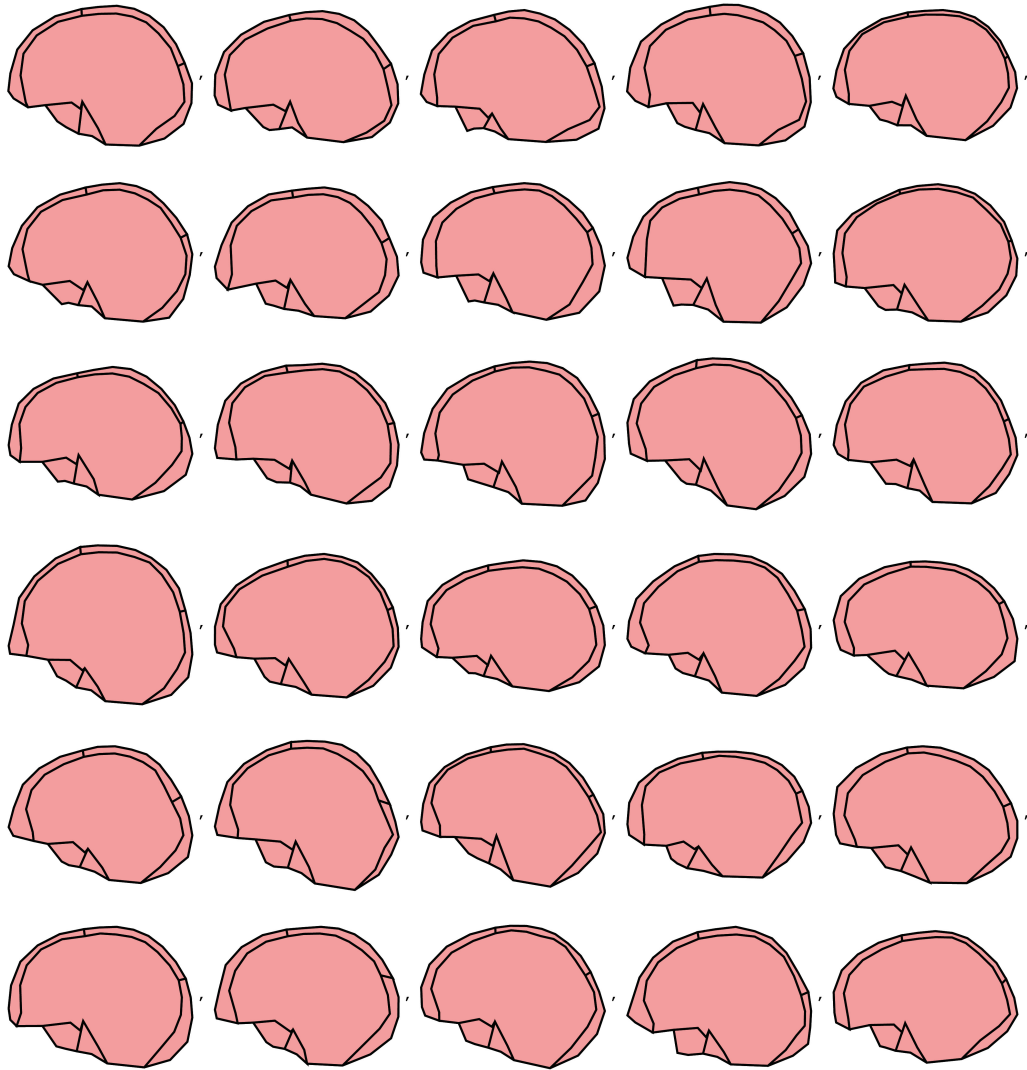
Figure 7: All individuals' neurocrania visualized as polygons for size analysis.

Table 6: Landmark assignments for shape analysis of the overall cranium.

structure	assigned landmarks
outline	54, 55, 56, 57, 58, 60, 62, 64, 1, 3, 5, 7, 9, 11, 13, 15, 17, 19, 21, 23, 25, 26, 33, 30, 38, 45, 47, 49, 51, 53, 44, 43, 42
frontal	1, 64, 62, 60, 58, 57, 56, 41, 40, 59, 61, 63, 65, 2
parietal	1, 3, 5, 7, 9, 11, 13, 15, 16, 14, 12, 10, 8, 6, 4, 2
occipital	15, 17, 19, 21, 23, 25, 26, 33, 30, 27, 32, 26, 25, 24, 22, 20, 18, 16
sphenoid	27, 29, 28, 39, 31, 34, 30
vomer	31, 35, 36, 37, 42, 52, 50, 48, 46, 45, 38, 30, 34
ethmoid	41, 40, 39
maxilla	42, 43, 44, 53, 51, 49, 47, 45, 46, 48, 50, 52
nasal cavity	54, 41, 39, 31, 35, 36, 37, 42
nasal	54, 55, 56
braincase	41, 40, 59, 61, 63, 65, 2, 4, 6, 8, 10, 12, 14, 16, 18, 20, 22, 24, 25, 26, 32, 27, 29, 28, 39

Table 7: Landmark assignments for shape analysis of the viscerocranium.

structure	assigned landmarks
viscerocranial outline	56, 55, 54, 42, 43, 44, 53, 51, 49, 47, 45, 38, 30, 33, 26, 32, 27, 29, 28, 39, 41, 40
frontal (for viscerocranium)	56, 41, 40
clivus	26, 32, 27, 30, 33
sphenoid	27, 29, 28, 39, 31, 34, 30
vomer	31, 35, 36, 37, 42, 52, 50, 48, 46, 45, 38, 30, 34
ethmoid	41, 40, 39
maxilla	42, 43, 44, 53, 51, 49, 47, 45, 46, 48, 50, 52
nasal cavity	54, 41, 39, 31, 35, 36, 37, 42
nasal	54, 55, 56

Figure 8: All individuals visualized as polygons for shape analysis.

Figure 9: All individuals' viscerocrania visualized as polygons for shape analysis.

Table 8: Landmark assignments for shape analysis of the neurocranium.

structure	assigned landmarks
neurocranial outline	56, 57, 58, 60, 62, 64, 1, 3, 5, 7, 9, 11, 13, 15, 17, 19, 21, 23, 25, 26, 33, 30, 34, 31, 39, 41
frontal	1, 64, 62, 60, 58, 57, 56, 41, 40, 59, 61, 63, 65, 2
parietal	1, 3, 5, 7, 9, 11, 13, 15, 16, 14, 12, 10, 8, 6, 4, 2
occipital	15, 17, 19, 21, 23, 25, 26, 33, 30, 27, 32, 26, 25, 24, 22, 20, 18, 16
sphenoid	27, 29, 28, 39, 31, 34, 30
ethmoid	41, 40, 39
braincase	41, 40, 59, 61, 63, 65, 2, 4, 6, 8, 10, 12, 14, 16, 18, 20, 22, 24, 25, 26, 32, 27, 29, 28, 39
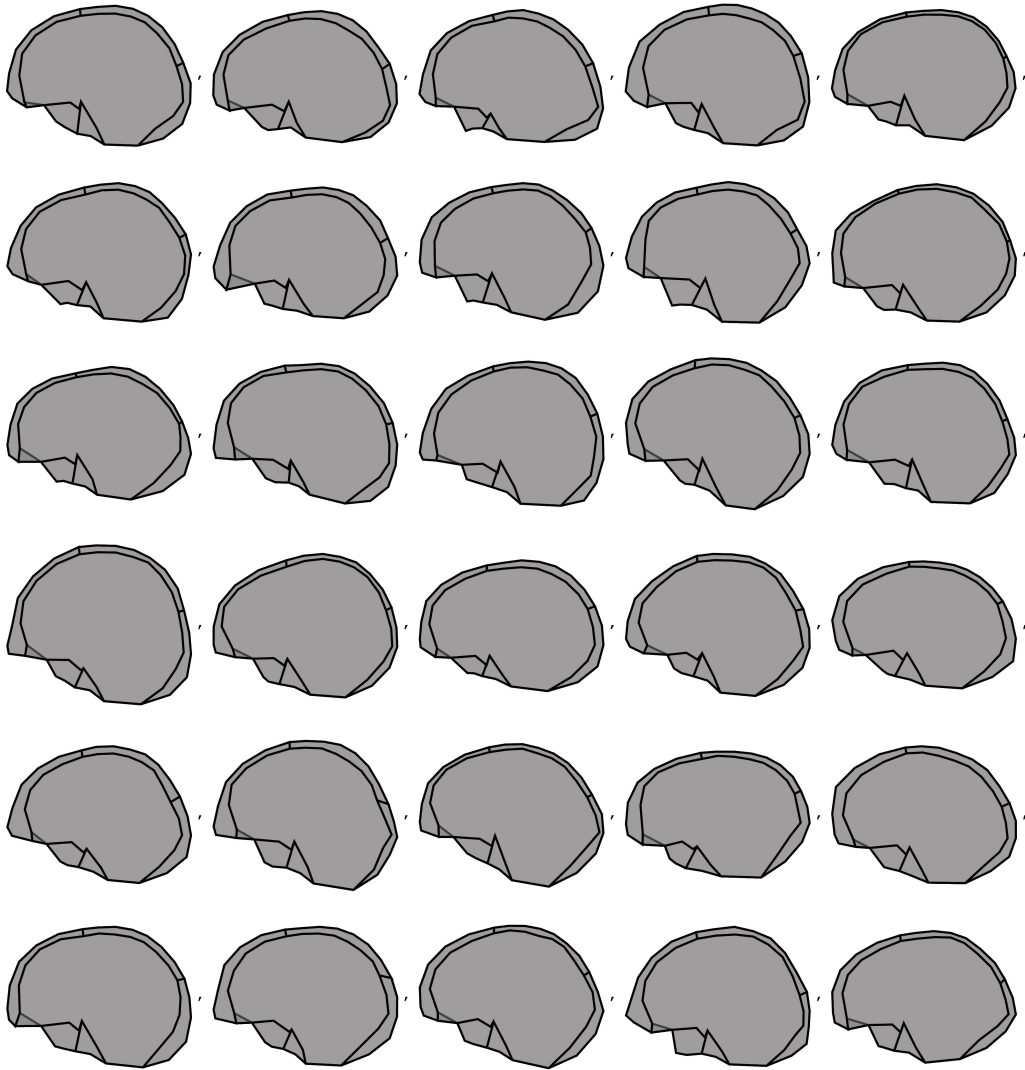
Figure 10: All individuals' neurocrania visualized as polygons for shape analysis.

5   Results

5.1   Principal Components

PC 1 showed that humans with high skulls also tend to have high faces, while humans with long skulls tend to have low faces. Moreover, PC 1 showed changes in the vomer and occipital (Fig. 11). PC 2 showed changes in the neurocranium, while the facial height remains about the same (Fig. 12). PC 3 showed changes in the vomer (Fig. 13). PC 4 showed changes in the forehead, maxilla and occipital (Fig. 14). PC 5 showed changes in the lower vomer, the maxilla and neurocranial thickness (Fig. 15). PC 6 showed changes in facial height and neurocranial thickness and angulation (Fig. 16). Plots for all principal components can be seen in Fig. 17.

5.2   Analysis of size

5.2.1   Overall cranium

The area variances of all individual bones and the overall cranial outline can be seen in Tab. 9 and Fig. 18A. The area variance for the entire median sagittal skull plane was $1.90 \times 10^4 cm^2$, while the sum of area variances of all other bones was $1.06 \times 10^4 cm^2$. The overall variance was clearly larger than the sum of individual variances. The quotient of the area variances divided by the area means for all structures ranged from 94.40 to 10.29 (Tab. 10 and Fig. 18B), but they were not the same for all bones. In the regression of the log-transformed area variances on the log-transformed area means the resulting regression slope was $+1.38$ (Fig. 19).

### 5.2.2   Viscerocranium

The results were similar for the viscerocranium. The area variances of all individual bones and the viscerocranial outline can be seen in Tab. 11 and Fig. 20A. The area variance for the entire median sagittal viscerocranial plane was $1890.15 cm^2$, while the sum of area variances of all other bones was $911.09 cm^2$. The overall variance was again visibly larger than the sum of individual variances. The quotient of the area variances divided by the area means for all structures ranged from 55.37 to 10.29 (Tab. 12 and Fig. 20B), but they were not the same for all bones. In the regression of the log-transformed area variances on the log-transformed area means the resulting regression slope was $+1.45$ (Fig. 21).

5.2.3   Neurocranium

For the neurocranium I once more found similar results. The area variances of all individual bones and the neurocranial outline can be seen in Tab. 13 and Fig. 22A. The area variance for the entire median

sagittal neurocranial plane was $1.31 \times 10^4 cm^2$, while the sum of area variances of all other bones was $9852.44cm^2$. The overall variance was larger than the sum of individual variances. The quotient of the area variances divided by the area means for all structures ranged from 74.49 to 10.29 (Tab. 14 and Fig. 22B), but they were not the same for all bones. In the regression of the log-transformed area variances on the log-transformed area means the resulting regression slope was +1.40 (Fig. 23).

5.3   Analysis of shape

5.3.1   Overall cranium

The shape variance for the entire cranial median sagittal outline (0.0054) was relatively small in comparison with the the other bones' shape variances, ranging from 0.0032 to 0.0361 (Tab. 15 and Fig. 24). In the regression of the log-transformed shape variances on the log-transformed inverse bending energy the resulting regression slope was +0.85 (Fig. 25). It should be mentioned, however, that the sliding landmark algorithm reduces the variance of semilandmarks. When these were not included in the calculation, the regression slope became smaller. For an alternative calculation of the regression slope using only a subset of the shape variables see .

5.3.2   Viscerocranium

The shape variance for the viscerocranial median sagittal outline (0.0151) was also relatively small in comparison with the the other bones' shape variances, ranging from 0.0072 to 0.0709 (Tab. 16 and Fig. 26). In the regression of the log-transformed shape variances on the log-transformed inverse bending energy the resulting regression slope was +0.92 (Fig. 27).

5.3.3   Neurocranium

The shape variance for the neurocranial median sagittal outline (0.0048) was again relatively small in comparison with the the other bones' shape variances, ranging from 0.0032 to 0.0361 (Tab. 17 and Fig. 28). In the regression of the log-transformed shape variances on the log-transformed inverse bending energy the resulting regression slope was +0.82 (Fig. 29).
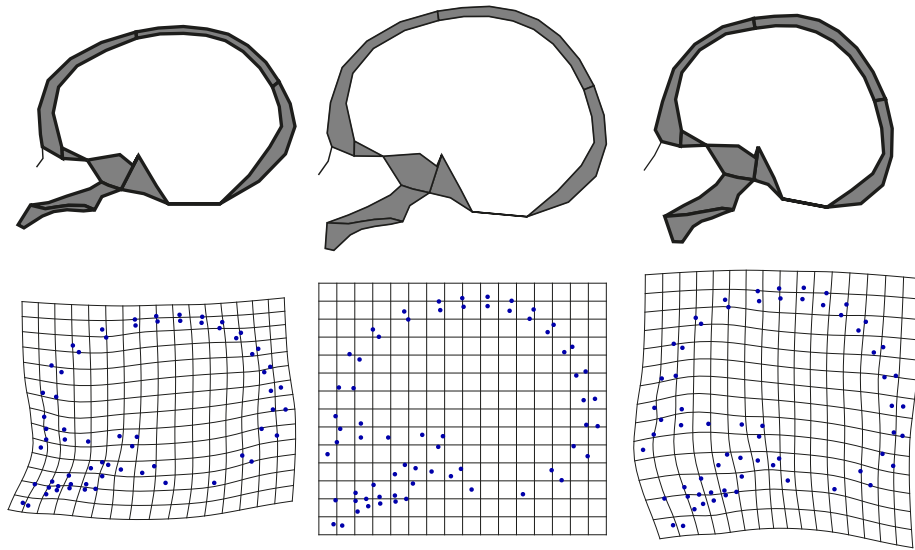
Figure 11: Top row: visualizations of principal shape component 1 (PC 1) as polygons. Bottom row: visualizations of PC 1 as deformation grids. Middle: mean shape. Left: negatively extrapolated shape along PC 1. Right: positively extrapolated shape along PC 1.
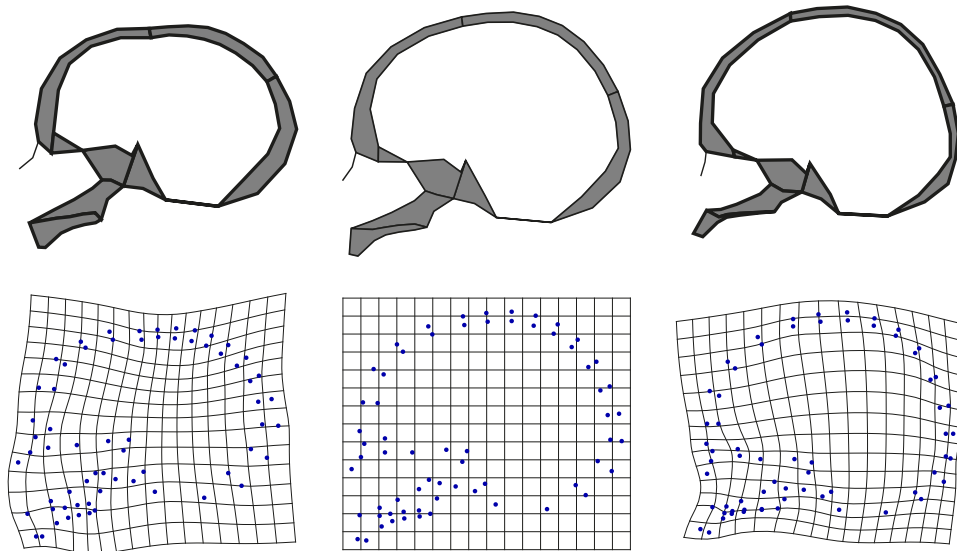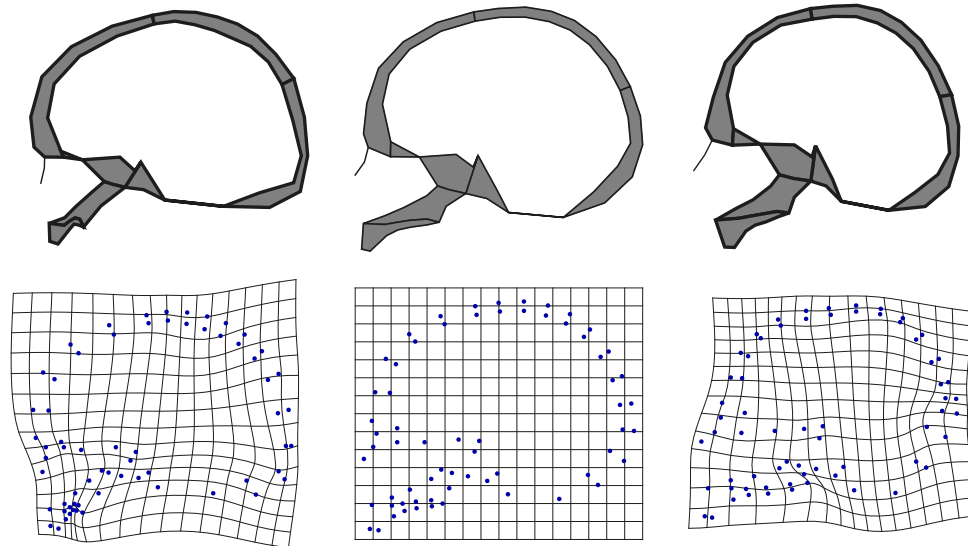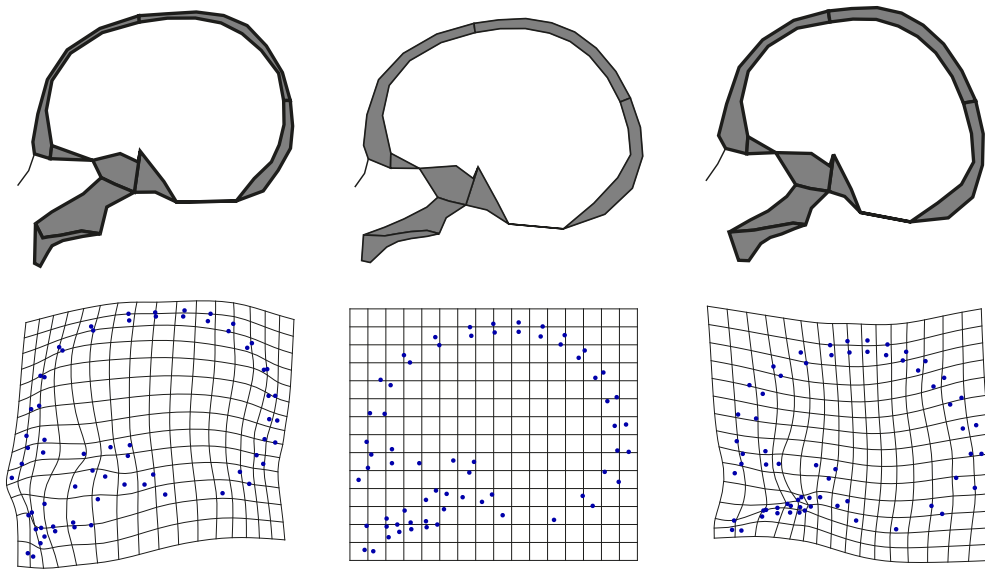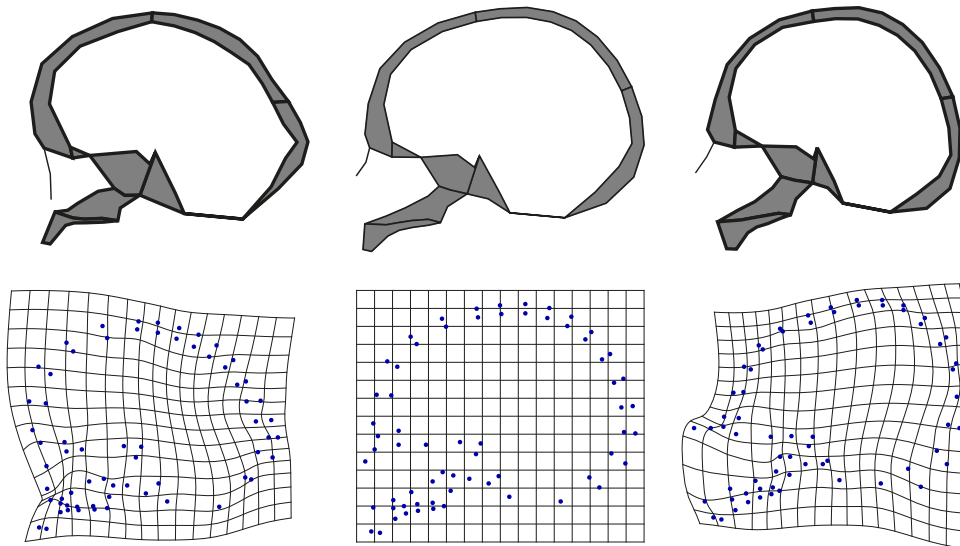

Figure 12: Top row: visualizations of principal shape component 2 (PC 2) as polygons. Bottom row: visualizations of PC 2 as deformation grids. Middle: mean shape. Left: negatively extrapolated shape along PC 2. Right: positively extrapolated shape along PC 2.
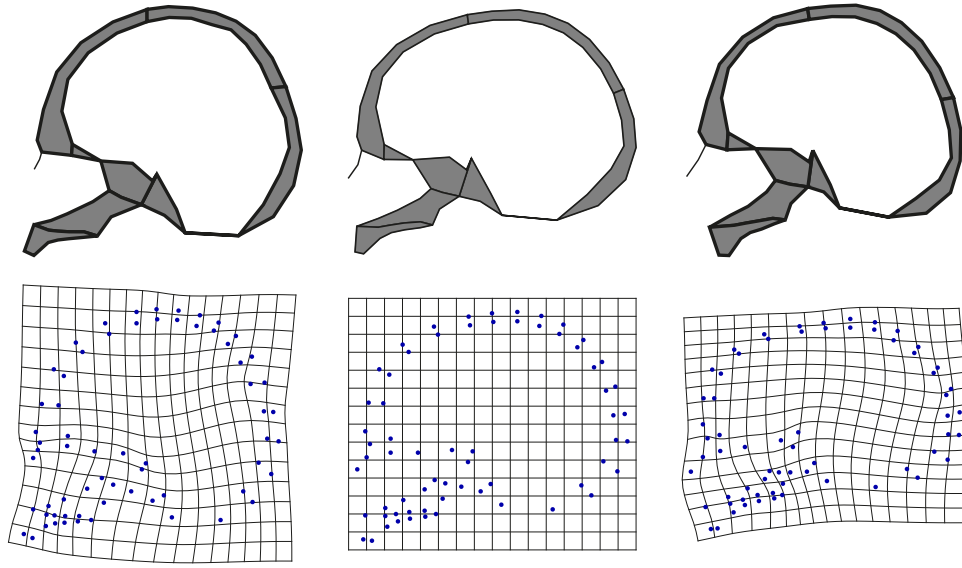
Figure 13: Top row: visualizations of principal shape component 3 (PC 3) as polygons. Bottom row: visualizations of PC 3 as deformation grids. Middle: mean shape. Left: negatively extrapolated shape along PC 3. Right: positively extrapolated shape along PC 3.

Figure 14: Top row: visualizations of principal shape component 4 (PC 4) as polygons. Bottom row: visualizations of PC 4 as deformation grids. Middle: mean shape. Left: negatively extrapolated shape along PC 4. Right: positively extrapolated shape along PC 4.

Figure 15: Top row: visualizations of principal shape component 5 (PC 5) as polygons. Bottom row: visualizations of PC 5 as deformation grids. Middle: mean shape. Left: negatively extrapolated shape along PC 5. Right: positively extrapolated shape along PC 5.

Figure 16: Top row: visualizations of principal shape component 6 (PC 6) as polygons. Bottom row: visualizations of PC 6 as deformation grids. Middle: mean shape. Left: negatively extrapolated shape along PC 6. Right: positively extrapolated shape along PC 6.
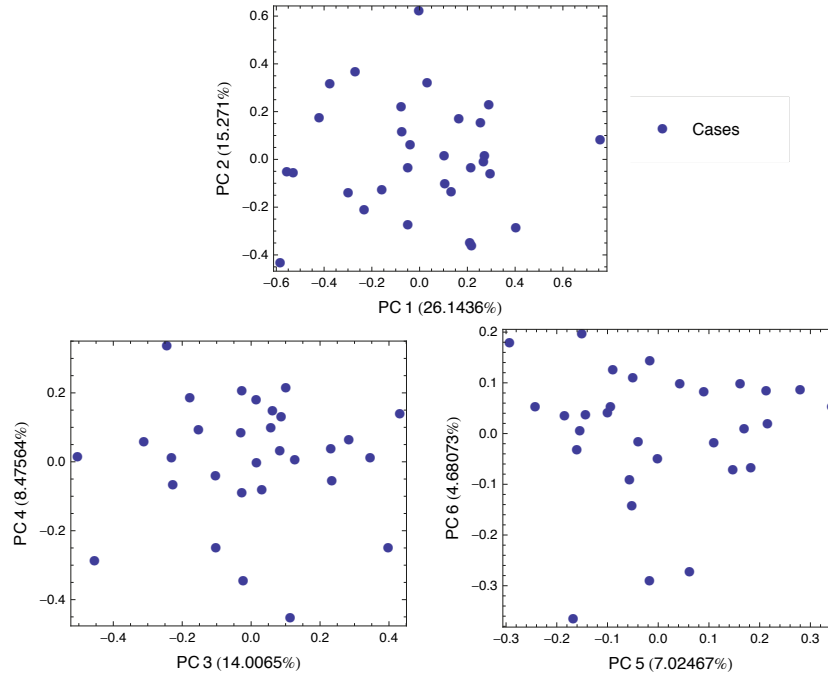
Figure 17: Plots for all principal components.

Table 9: Area variances of the overall cranium for size analysis.

structure	area variance (in cm^2)
outline	$1.90{\times}10^4$
sum of individual bones	$1.06{\times}10^4$
frontal	335.30
parietal	214.95
occipitalpart	273.21
clivus	35.32
sphenoid	81.70
vomer	205.39
maxilla	60.09
nasal cavity	506.90
pseudonasal	21.69
braincase	8912.00

Table 10: Area variances divided by area means of the overall cranium for size analysis.

| structure	area variance / area mean
outline	94.40
frontal	32.24
parietal	28.79
occipitalpart	33.30
clivus	10.29
sphenoid	14.65
vomer	34.81
maxilla	17.21
nasal cavity	35.15
pseudonasal	16.43
braincase	63.28
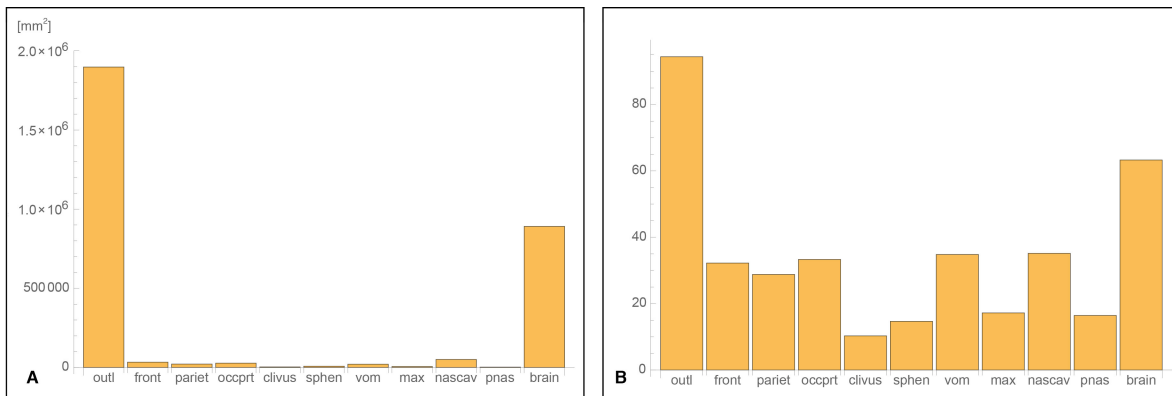
Figure 18: (A) Area variances of the overall cranium for size analysis. (B) Area variances divided by area means of the overall cranium for size analysis. Captions: outl = outline, front = frontal, pariet = parietal, occprt = occipitalpart, clivus = clivus, sphen = sphenoid, vom = vomer, max = maxilla, nascav = nasal cavity, pnas = pseudonasal, brain = braincase.
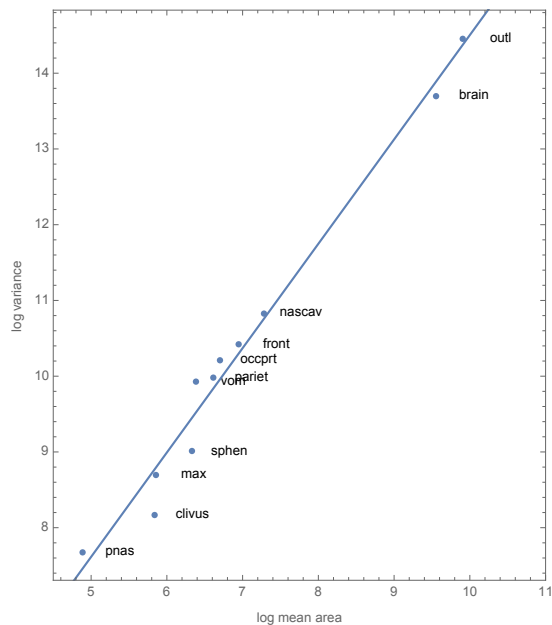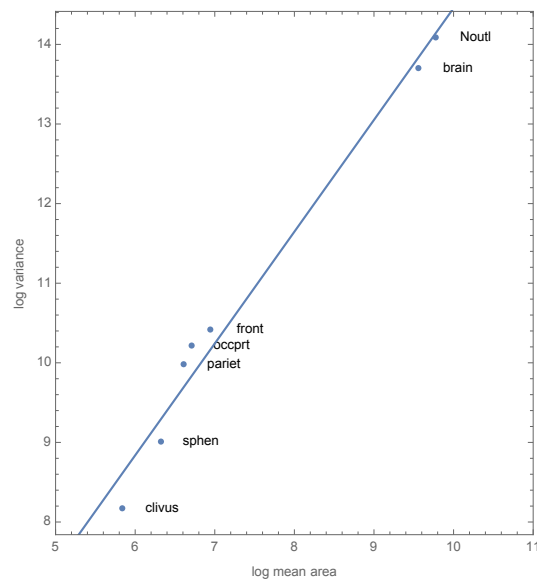
Figure 19: Log area variances regressed on log mean area of the overall cranium for size analysis. Regression slope $= +1.38$.

Table 11: Area variances of the viscerocranium for size analysis.

structure	area variance (in cm^2)
viscerocranial outline	1890.15
sum of individual bones	911.09
clivus	35.32
sphenoid	81.70
vomer	205.39
maxilla	60.09
nasal cavity	506.90
pseudonasal	21.69

Table 12: Area variances divided by area means of the viscerocranium for size analysis.

structure	area variance / area mean
viscerocranial outline	55.37
clivus	10.29
sphenoid	14.65
vomer	34.81
maxilla	17.21
nasal cavity	35.15
pseudonasal	16.43
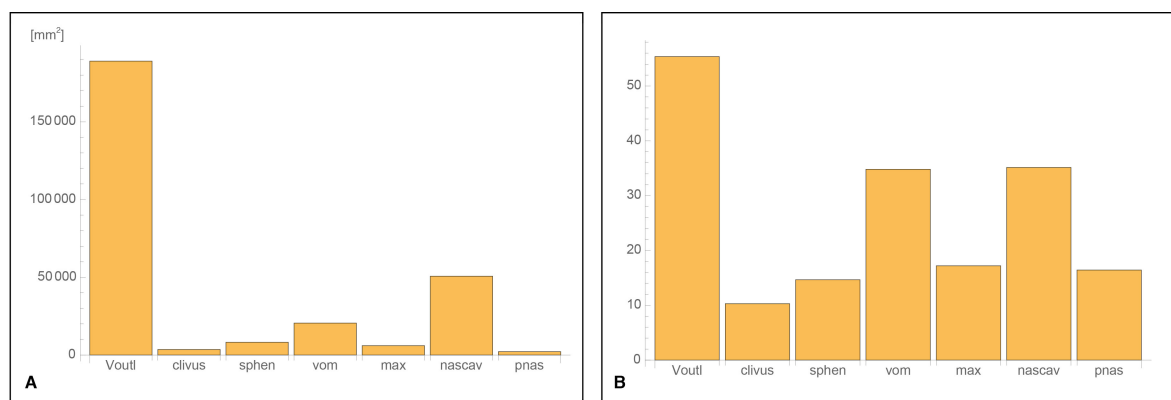
Figure 20: (A) Area variances of the viscerocranium for size analysis. (B) Area variances divided by area means of the viscerocranium for size analysis. Captions: Voutl = viscerocranial outline, clivus = clivus, sphen = sphenoid, vom = vomer, max = maxilla, nascav = nasal cavity, pnas = pseudonasal.
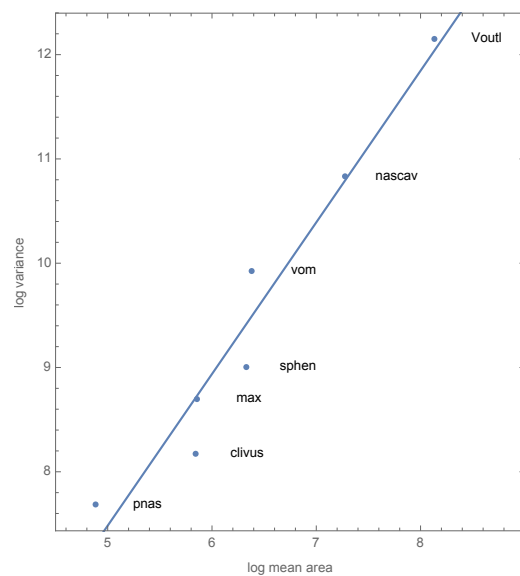
Figure 21: Log area variances regressed on log mean area of the viscerocranium for size analysis. Regression slope = +1.45.

Table 13: Area variances of the neurocranium for size analysis.

structure	area variance (in cm^2)
neurocranial outline	$1.31x10^4$
sum of individual bones	9852.44
frontal	335.28
parietal	214.95
occipitalpart	273.21
clivus	35.32
sphenoid	81.70
braincase	8912.00.

Table 14: Area variances divided by area means of the neurocranium for size analysis.

structure	area variance / area means
neurocranial outline	74.49
frontal	32.24
parietal	28.79
occipitalpart	33.30
clivus	10.29
sphenoid	14.65
braincase	63.28
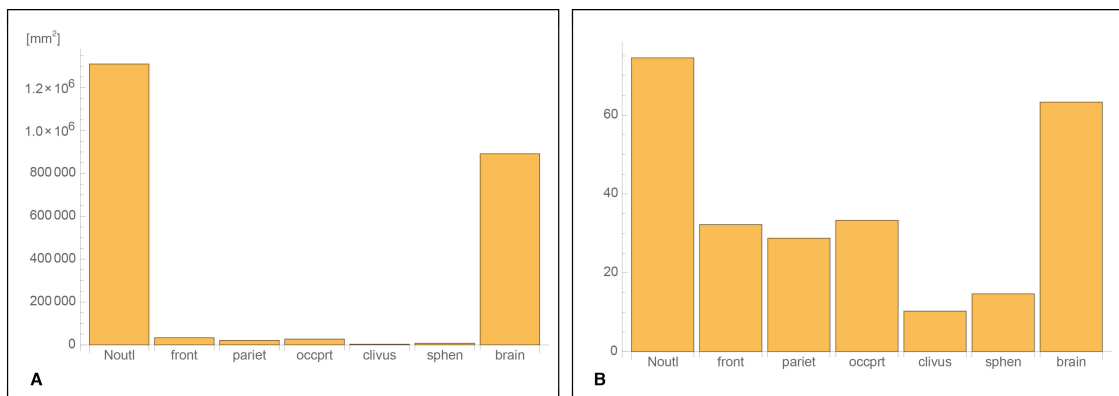
Figure 22: (A) Area variances of the neurocranium for size analysis. (B) Area variances divided by area means of the neurocranium for size analysis. Captions: Noutl = neurocranial outline, front = frontal , pariet = parietal, occprt = occipitalpart, clivus = clivus, sphen = sphenoid, brain = braincase.

Figure 23: Log area variances regressed on log mean area of the neurocranium for size analysis. Regression slope = +1.40.

Table 15: Shape variances of the overall cranium for shape analysis.

structure	shape variance
outline	0.0054
frontal	0.0056
parietal	0.0032
occipital	0.0076
sphenoid	0.0361
vomer	0.0312
ethmoid	0.0261
maxilla	0.0294
nasal cavity	0.0289
nasal	0.0072
braincase	0.0057
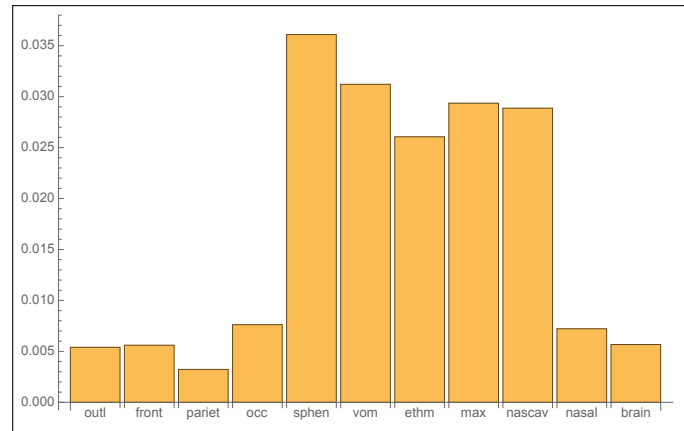
Figure 24: Shape variances of the overall cranium for shape analysis. Captions: outl = outline, front = frontal, pariet = parietal, occ = occipital, sphen = sphenoid, vom = vomer, ethm = ethmoid, max = maxilla, nascav = nasal cavity, nasal = nasal, brain = braincase.
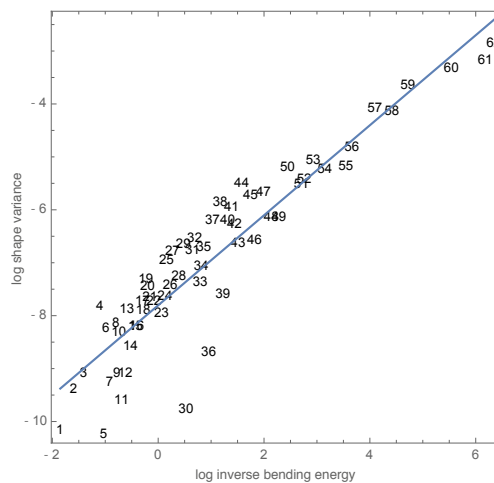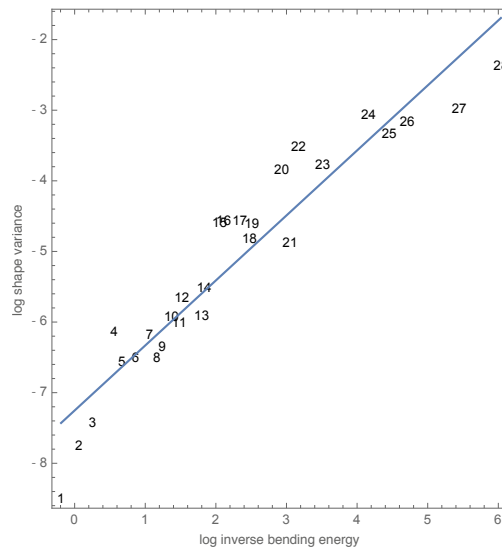

Figure 25: Log shape variances regressed on log inverse bending energy of the overall cranium for shape analysis. Regression slope = +0.85.

Table 16: Shape variances of the viscerocranium for shape analysis.

structure	shape variance
viscerocranial outline	0.0151
frontal (for viscerocranium)	0.0709
clivus	0.0201
sphenoid	0.0361
vomer	0.0312
ethmoid	0.0261
maxilla	0.0294
nasal cavity	0.0289
nasal	0.0072
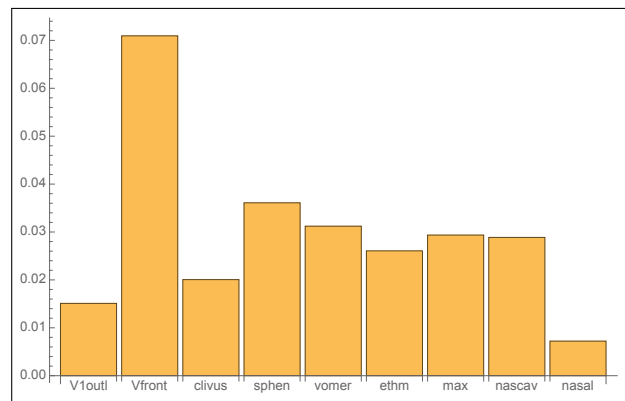
Figure 26: Shape variances of the viscerocranium for shape analysis. Captions: V1outl = viscerocranial outline (for shape analysis), Vfront = frontal (for viscerocranium), clivus = clivus, sphen = sphenoid, vomer = vomer, ethm = ethmoid, max = maxilla, nascav = nasal cavity, nasal = nasal.

Table 17: Shape variances of the neurocranium for shape analysis.

structure	shape variance
neurocranial outline	0.0048
frontal	0.0056
parietal	0.0032
occipital	0.0076
sphenoid	0.0361
ethmoid	0.0261
braincase	0.0057

Figure 27: Log shape variances regressed on log inverse bending energy of the viscerocranium for shape analysis. Regression slope = +0.92.
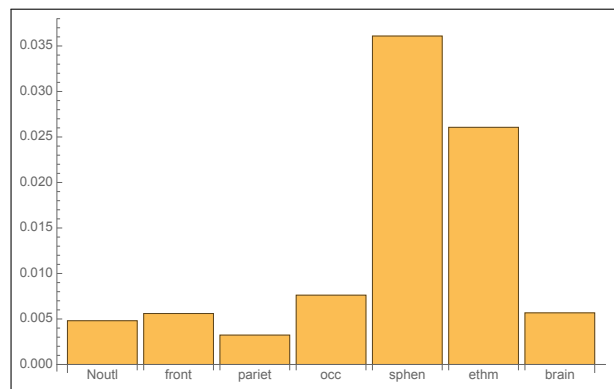
Figure 28: Shape variances of the neurocranium for shape analysis. Captions: Noutl = neurocranial outline, front = frontal, pariet = parietal, occ = occipital, sphen = sphenoid, ethm = ethmoid, brain = braincase.
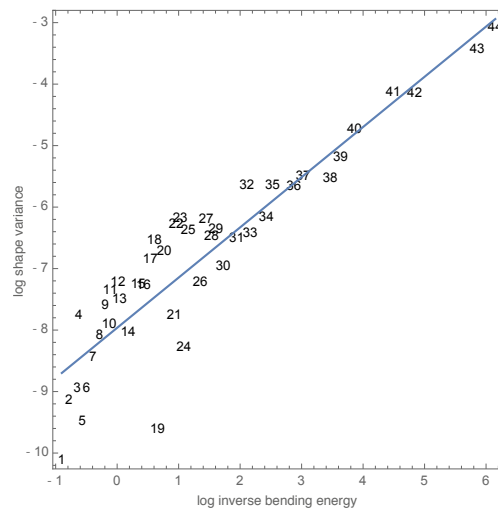
Figure 29: Log shape variances regressed on log inverse bending energy of the neurocranium for shape analysis. Regression slope = +0.82.

6 Discussion

In the analysis of size, the overall area variance was larger than the sum of the individual bones' variances. This was the same for the overall cranium, the viscerocranium and the neurocranium. In terms of our toy model, the overall variance was larger than the sum of the individual bones' variances plus twice their pairwise covariances; this means that the net covariance between the bones was positive and thus the individual bones were positively correlated. Therefore, bone size within the cranium, and also within the viscero- and neurocranium, seems to be directed via 'coordinated growth'. Moreover, the regression slopes for the log-transformed area variances and the log-transformed mean areas, for the cranium as well as its two partitions, were distinctly larger than 1. This, again, is an indicator for 'coordinated growth' between the bones. Since for none of the cranial definitions the quotients of the individual area variances divided by their respective means were equal among all of the structures' parts, one can further see that the pairwise covariances between the bones do not cancel each other out. Instead, it seems that the individual bones' sizes are dominantly controlled via a process of 'coordinated growth'. This means that if one part grows bigger, the other parts will grow bigger too and if one part grows to be smaller, the other parts will be smaller too.

This finding can, for example, be explained by allometry. Skulls, as well as the remaining human body, vary greatly in overall size. To still form a functional whole, the parts of a larger overall structure must also be large, while the parts of a smaller structure must be small.

In the analysis of shape, the overall shape variance was relatively small compared to the other bones of the cranium. As the individual shapes do no not add up to the overall shape, one cannot infer solely from this finding that 'compensatory growth' is operative. One can, however, clearly see that the individual bone shapes were much more variable than the overall cranial shape. To make inferences about the nature of growth, the regression slopes for the log-transformed variances and the log-transformed inverse bending energy have to be considered. All three slopes were smaller than 1. This finding, albeit not as striking as the one for size, indicates that what Bookstein (2015) called 'disintegration' and what in the terminology of this thesis is called 'compensatory growth' is the dominating process for controlling individual bone shape. This means that the individual bone shapes are negatively correlated and grow in a way that compensates for shape that diverges from the mean. Thus, if one part grows to be more concave, the adjacent part will grow to be more convex, for example, if they need to grow into an 'integrated' whole.

This finding can be explained by 'canalization' at the level of overall shape. Cranial shape seems to be 'canalized' through stabilizing selection or developmental constraints. To shape a functioning whole, the individual parts have to correct each other's inaccuracies, i.e. compensate for each other.

From these observations logically follows the question why shape is 'canalized', while size is not.

Could it be that shape is more important for function than size? This seems plausible, if we consider crania of different sizes. Regardless of their size, they will enable a person to breathe and chew – as long as the shapes of the facial and jaw bones fit together and form an overall functioning whole. Only if the overall shape of the structure is preserved, can the innate function be optimally performed. To theorize about how these 'coordinated' and 'compensatory growth' processes occur within the cranium, we first have to consider the histology and mechanobiology of bones.

6.1   Bone histology

Bone is a composite material made up of organic compounds (mostly collagen) and inorganic mineral crystals (mostly hydroxyapatite). This combination of rigid and resilient materials gives bone its strength. According to the densitiy of bone, two types can be distinguished. Cortical bone is denser and usually encompasses the more porous trabecular bone. Spread over the exterior surface of bone is a tissue called periosteum. Underneath it there is a high concentration of cell types called osteoblasts. These are bone-forming cells that synthesize and deposit osteoid, a collagen-rich material. When crystals are deposited into the osteoid, the osteoblasts become trapped within lacunae in the bony matrix; they are now called osteocytes. The osteocytes are connected via microscopic fluid-filled channels called caniculi. Through these caniculi the osteocytes obtain the nutrients they need to maintain the bone tissue. Cells of a different type, the osteoclasts, remove bony matrix. They are situated in Howship's lacunae on the bone surface (Mays 1998; White and Folkens 2005).

A distinction is often made between the initial growth of bone and the continuous bone removal and substitution throughout life. The former is usually referred to as 'modeling' and the latter as 'remodeling'. Furthermore, two types of bone modeling can be identified, according to the original material that is being replaced by bony matrix (Mays 1998; White and Folkens 2005). Both are initiated by a proliferation of mesenchymal cells which are then differentiated into chondroblasts or osteoblasts (Hall 2015). For endochondral ossification, chondroblasts first build cartilage which is, later on, substituted with bony tissue by osteoblasts. For intramembraneous or dermal ossification, the mesenchymal cells differentiate into osteoblasts which build bone directly. Multiple ossification centers can form within the tissue and later fuse together (Mays 1998; White and Folkens 2005; Junqueira and Carneiro 2005; Ankel-Simons 2007; Hall 2015). Endochondral as well as intramembraneous bone can be found within the cranium. Ontogenetically, the chondrocranium, consisting of endochondral bones, appears first from capsules that hold the eyes, ears, nose and cranial base. Dermal bones are then added (Ankel-Simons 2007; Hall 2015). Among the bones that concern us in this thesis, endochondral bones are (most of) the occipital, (most of) the sphenoid, parts of the temporal and the ethmoid and dermal bones are the nasal, the vomer, the palate, the frontal, the maxilla, parts of the temporal, part

of the sphenoid, part of the occipital and the parietal (Ankel-Simons 2007; White and Folkens 2005).

6.2   Bone mechanobiology

Skeletal mechanobiology is based on the assumption that the morphology of skeletal elements, such as bone and cartilage, is susceptible to mechanical forces acting on them and physically adapts to the stress it is exposed to (Meulen and Huiskes 2002). "Mechanotransduction describes the cellular processes that translate mechanical stimuli into biochemical signals, thus enabling cells to adapt to their physical surroundings" (Jaalouk and Lammerding 2009). The idea that the internal and external composition of bone is influenced by mechanical forces was first made public by Julius Wolff (1892 as cited in Frost 1998) and is now known as Wolff's law. It was further developed by Frost (1987; 1998; 2003) over the past decades. He proposed a homeostatic mechanism, called a 'mechanostat'. This mechanism monitors whether bone mass corresponds to the amount of usage it experiences by comparing the actually experienced strain to the 'minimum effective strain' (MES), a threshold point. If the mechanical strain is greater than the MES, more bone mass will be formed. Whereas, if the mechanical strain is less than the MES, bone will be resorbed. Moreover, the mechanostat hypothesis also incorporates other influences on remodeling such as "local nonmechanical agents (genes, cytokines, ligands, receptors, paracrine and autocrine effects, apoptosis, etc.)" and "systemic, blood-borne non-mechanical agents (hormones, minerals, vitamins, drugs, nutrients, etc.)" (Frost 2003).

Kahn and Partridge (1991) proposed that there are three possibilities for the initiation of bone remodeling: the resorption of calcium into the blood stream, the repair of tiny fractures within the bone and the adaptation to mechanical force. They further suggested that osteoblasts sense mechanical force and start the remodeling process. They hypothesized that osteoblasts could either sense changes in mechanical force instantly via stretch receptors in their membrane or react to a 'stress generated potential' arising between the bone tissue and the blood vessels. Chambers (1991) contributed that osteoblasts can communicate using long cell processes.

Burger and Klein-Nulend (1999) have further explored these ideas. They reviewed evidence that osteocytes are the mechanosensory cells and proposed "that the combination of cellular network and lacuno-canalicular porosity performs the functions of mechanosensing and mechanotransduction in bone": "When bone is loaded, interstitial fluid is squeezed through the thin layer of non-mineralized matrix surrounding cell bodies and cell processes toward the Haversian or Volkmann channels, thereby producing fluid shear stress at the osteocyte cell membrane" (Burger and Klein-Nulend 1999). The thusly activated osteocytes then synthesize anabolic paracrine factors which are transported to osteoblasts in the periosteum through the lacuno-canicular porosity. In case of lower than usual mechanical load, i.e. disuse, osteocyte shear-stress as well as the delivery of nutrients to the osteocytes and

transport of waste products from the osteocytes is reduced. This could initiate osteocyte apoptosis, which could activate osteoclasts (Burger and Klein-Nulend 1999). Similar to Frost's (1987; 1998; 2003) mechanostat hypothesis, Burger and Klein-Nulend (1999) concluded that bone is built and resorbed in response to use and disuse so that a steady state of force per bone mass is preserved. This idea was also described by Skerry (2000; 2003), who moreover detailed a cascade of signals that is induced in bone when it is mechanically loaded: mechanical deformation causes a calcium influx in osteoblasts, succeeded by an activation of messenger pathways and gene expression of (among others) transforming growth factor β (TGFβ), insulin-like growth factor I (IGF-I) and type-I-collagen and, finally, markers for bone resorption are inhibited, while osteoblasts are stimulated (Skerry 2000). Ruimerman and Huiskes (2005) and Huiskes et al. (2000) also proposed a homeostatic remodeling process. They put forth a unifying theory that explains how the density and direction of bone architecture adapts to mechanical strains it is exposed to. In conclusion, it is widely accepted that increased strain causes deformations in bone which induce a signaling cascade initiating bone growth.

6.3   Implications for cranial development

There are various examples for how the reactivity of bone to mechanical forces influences bone formation and development. One of the most striking examples are the artificial skull deformations that have been practiced worldwide since prehistoric times, albeit, nowadays, only in ameliorated form (Teschler-Nicola and Mitteroecker 2007). These artificial deformations show without a doubt that mechanical strain, when applied to the cranium, can result in remarkable aberrations from mean cranial shape and that changes in one skull area also impact the other areas. Another example is the well known phenomenon of bone loss in astronauts in space. Burger and Klein-Nulend (1999) hypothesized that the low gravity environment decreases weight and the volume of contractile muscle force impacting the bone and thereby lacuno-canicular fluid flow is reduced. Simply put, the weightless environment mirrors a situation of disuse which the bones react to with osteoclastic activity.

The results of this thesis show that overall shape within the human cranium is achieved via 'compensatory growth' processes between the individual bones. Another instance where 'compensatory growth' is evident within the skull as well as within the remaining skeleton is fluctuating asymmetry (FA). Kellner and Alford (2003) found that in domestic foul patterns of FA were shaped by corrective mechanisms in bone growth where 'compensatory growth' increases and decreases growth on opposing sides to even out imbalances. Hallgrímsson (1999) studied FA in *Macaca mulatta* and *Homo sapiens* and found that the variance of FA increased during ontogeny. They concluded that two models could account for the increasing variance: The morphogenetic drift model states that either local growth regulation becomes more variable or undirected bone remodeling leads to a more variable bone shape.

Both scenarios assume that intrinsic factors play a major role in bone development. The functional asymmetry hypothesis, on the other hand, states that asymmetric epigenetic factors, such as an uneven gait or other mechanical loading of bone, lead to accumulation of variation. Hallgrímsson (1999) furthermore suggested that the ontogenetic increase in FA variance could be based on reduced stability in the development of the skeleton which, in turn, "could be a cost in the evolution of prolonged growth periods".

This raises the question whether such developmental instability is the reason for the high shape variance of individual skull bones in comparison to the overall skull shape. Since the overall cranial shape shows so little variance, some stabilizing processes must be active there, however. A similar idea was proposed by Paul Weiss in a conference transcript (as cited in Gerard 1958). He stated that "the total process has a greater degree of invariance than the individual component parts" and gave an example: "Identical twins are much more similar than are any microscopic sections from corresponding sites you can lay through either of them". Even in a genetically identical setting, developmental processes are variable and lead to phenotypic differences between corresponding parts, while the overall phenotype remains remarkably stable.

Zelditch et al. (2006) suggested that covariation patterns within the skull are changed throughout ontogeny by processes that reduce variance, i.e. by 'canalizing' processes, because skull variation remains constant during ontogeny, while the bone structures are constantly altered. They concluded that 'compensatory growth' processes create and remove variance at the same rate so that overall variance remains constant. They further stated that there are two possibilities for the regulation of cranial shape: either cranial shape is actively monitored and regulated so that bone deposition and resorption are active corrective responses to deviations from a given shape, or strain is "regulated so that deviations from the normal shape are incidentally corrected when bone adapts to local strains" (Zelditch et al. 2006). In the first scenario, the overall product of developmental processes, in this case the cranium, is 'canalized', evolved possibly through stabilizing selection. In the second scenario, mechanical forces do not directly 'canalize' cranial shape. Instead, the amount of strain per bone mass is the variable under regulation and thus gene expression and products are regulated via epigenetic mechanisms (Zelditch et al. 2004; Zelditch et al. 2006). Just as Hallgrímsson (1999) suggested in his functional asymmetry hypothesis [1], Zelditch et al. (2004) proposed that asymmetrical interactions between bone and soft tissue result in fluctuations of symmetry and necessitate 'compensatory' development between the bones. These compensations are directed by regulating the strain that soft tissues will put on bony structures, i.e. by keeping it at a steady rate. As other authors have maintained that bone remodeling is triggered when strain exceeds or falls below a strain threshold, so that a

---

[1]Zelditch et al. (2004) in fact referred to the morphogenetic drift hypothesis which was mentioned in the same paper (Hallgrímsson 1999), but it is clear from the context that the functional asymmetry hypothesis was meant.

steady rate of strain per bone mass at the threshold level is achieved (Frost 1987; Frost 1998; Frost 2003; Burger and Klein-Nulend 1999; Skerry 2000; Skerry and Suva 2003; Ruimerman and Huiskes 2005; Huiskes et al. 2000), it is possible that this mechanism regulates cranial bone growth. Since the induction of cranial bone formation does not require mechanical forces (Hall 2015), initial bone growth must be genetically determined. Thus, the overall phenotype of cranial shape may only be prenatally regulated in so far as aberrations from the genetically determined normal initiation of bone modeling are eradicated by developmental constraints or stabilizing selection (Zelditch et al. 2004; Zelditch et al. 2006). All further 'canalization' of shape would then be regulated by epigentic processes that result in 'compensatory growth' between the bones (Zelditch et al. 2004; Zelditch et al. 2006). Hall (2015) observed that the original condensations define the bones' basic shape and size, while the further development of shape and cranial growth is highly influenced by mechanical forces. He further hypothesized that the cranial modeling and remodeling processes within the cranial sutures are not the primary growth force within the cranial vault, but that sutural growth responds to other influences.

Sources of mechanical interaction with bone are other bones, the brain and muscles. While cartilage bone growth is majorly driven by intrinsic factors (Opperman 2000; Hall 2015), dermal bone growth is very reliant on direct mechanical influences (Opperman 2000; Spector et al. 2002; Yu et al. 2001) and therefore susceptible to mechanical loadings from adjacent cartilage bones. Hallgrímsson et al. (2006) showed that cranial bones, due to their physical contact, impact their neighbors' growth and that the resulting variation originates in the cartilage bones and is transmitted to the remaining cranial bones. Thus it seems that pleiotropy influences groups of the same bone type and that physical contact between the bones causes epigenetic effects. These interactions between the two bone types, according to Hallgrimsson et al. (2007), are the key to understanding the development and change of cranial shape. Nonetheless, brain growth seems to be the most influential factor regarding the growth of the brain case (Hall 2015; Yu et al. 2001; Jiang et al. 2002). The membrane that encloses the brain, the dura mater, is probably at least partly fused with the periost of the cranial vault bones and can initiate osteogenesis (Hall 2015) and the brain gives molecular signals to regulate facial bone cell proliferation (Marcucio et al. 2005). Variation in these intrinsic developmental processes leads to variation in the end product and thereby covariaton (Hallgrímsson et al. 2009). The influence of muscles on cranial bones has also often been associated with covariance between them (e.g. Cheverud 1982; Willmore et al. 2006). Nowlan et al. (2008) found that cyclic muscle contractions activated osteoblasts and thereby bone formation in long bones of bird embryos. It therefore seems plausible to assert that strains induced by muscle activity could also augment cranial bone growth. Zelditch et al. (2004) proposed that muscle activity is already necessary in embryonic development for the production of

normal bones and Hallgrimsson et al. (2007) hypothesized that the influence of muscle activity will further rise with the onset of mastication.

If the final skull shape was not directly 'canalized', but incidentally achieved by epigenetic effects to regulate mechanical strain, it would follow that instead the initial formation and patterning of cranial bones as well as the genes impacted by the epigenetic mechanisms are 'canalized' by stabilizing selection. Moreover, these genes should be shared among bones, just as cranial bones that share the same mode of ossification should also share the same genetic regulation for that mode (Hallgrimsson et al. 2007) and therefore 'genetic integration' (Cheverud 1982; Cheverud 1996a; Cheverud 1996b) due to pleiotropy would cause covariation between the bones. Another source of covariation would stem from the shared origin of mechanical forces applied to the cranium, i.e. soft tissues such as the brain and muscles, apply strain to multiple bones (Zelditch et al. 2006); this would be an instance of 'environmental integration' (Cheverud 1982; Cheverud 1996a; Cheverud 1996b). If the final skull shape was not 'canalized', this would also explain how artificial skull deformations (Teschler-Nicola and Mitteroecker 2007) are possible: the genetic determinants of bone growth that are compatible with life are selected in utero and further growth of bone shape and size is determined by mechanical forces put on the skull, may they be naturally occurring forces generated by other tissues or artificial forces provided by external devices. Any mechanical forces or lack thereof could then be translated into bone growth or resorption via the signaling mechanisms detailed above (see section 6.2). If the final skull shape was directly 'canalized', on the other hand, then active correction in the amount of deposited or resorbed bone could be controlled via pleiotropy with opposing effects on different bones. Both scenarios would result in 'compensatory growth' between the bones and could therefore explain the findings of this thesis regarding shape.

For size, however, we detected 'coordinated growth'. This finding could be caused by pleiotropic gene expression. The original bone/cartilage condensations in the initial stage of bone formation and patterning should be 'genetically integrated' and the bones' basic size should thus be set (Hall 2015) by pleiotropic effects from the shared genes. Moreover, this allometric effect could be achieved by pleiotropic genes that cause 'coordinated growth' during ontogeny, growth hormones, etc.

These hypotheses can be tested by future studies in order to eventually understand the process of cranial growth regulation and the mechanotransductive pathways involved in it. Moreover, comparisons of these findings across species will unravel whether these mechanisms are conserved, when they emerged and possibly help determine the original developmental system that shifted to allow 'integrated' bone growth.

7 Supplement

7.1 Alternative bone definitions

As mentioned before (see section 4.2), alternatives for the sphenoid and the occipital were defined, since the closed suture between them had to be estimated. The 'sphenooccipital' is comprised of the sphenoid and the part of the occipital ventral of the foramen magnum, i.e. the clivus. The 'occipitalpart' is the part of the occipital posterior of the foramen magnum. Moreover, since some landmarks were more difficult to place on the sphenoid, and likewise on the 'sphenooccipital', alternatives were defined to test whether any of these landmarks influenced the results. All alternative landmark assignments can be seen in Tab. 18.

7.2 Results for size

7.2.1 Sphenooccipital alternatives as a substitute for the sphenoid and clivus

In the alternative size calculations the sphenoid and the clivus were substituted by the sphenooccipital. The area variances of all individual bones and the overall cranial outline can be seen in Tab. 19 and Fig. 30A. The area variance for the entire median sagittal skull plane was $1.90{\times}10^4 cm^2$, while the sum of area variances of all other bones was $1.07{\times}10^4 cm^2$. In the original calculation the sum of all area variances had been $1.06{\times}10^4 cm^2$. Therefore, the overall variance was still clearly larger than the sum of individual variances. The range of the quotients of the area variances divided by the area means had not changed (Tab. 20 and Fig. 30B) and thus they still were not the same for all bones. These results, moreover, did not change when one of the sphenooccipital alternatives was inserted instead of the sphenooccipital (Tab. 21, 22 and Fig. 31). The regression slopes of the log-transformed area variances regressed on the log-transformed area means for calculations with the sphenooccipital or its alternatives can be seen in (Fig. 32). In all cases the resulting regression slope was +1.33. In the original calculation the slope had been +1.38. In conclusion, the use of any of the sphenooccipital alternatives did not result in a different outcome; the results still support the conclusion that 'coordinated growth' is active in size regulation of the skull.

7.2.2 Sphenoid alternatives

In this alternative calculation the sphenoid was substituted by different alternatives. The area variances and quotients did not differ substantially between the sphenoid alternatives (Tab. 23, 24 and Fig. 33). In addition, the regression slopes of the log-transformed area variances regressed on the log-transformed area means were either +1.38, as in the original calculation, or +1.37 (Fig. 34). Thus, the use of any of the sphenoid alternatives did not result in a different outcome; the results still

support the conclusion that 'coordinated growth' is active in size regulation of the skull.

7.3 Results for shape

7.3.1 Sphenooccipital alternatives and occipitalpart as substitutes for the sphenoid and occipital

In this calculation the sphenoid and occipital were substituted by the sphenooccipital and the occipitalpart. The shape variances for both fell well into the range of the original calculation and were still far larger than the shape variance for the entire cranial outline (Tab. 25 and Fig. 35). The alternatives for the sphenooccipital did not change this outcome either (Tab. 26 and Fig. 36). In the regression of the log-transformed shape variances on the log-transformed inverse bending energy the resulting regression slope was +0.85 for all sphenooccipital alternatives paired with the occipitalpart (Fig. 38). Overall, the use of any of the alternatives did not result in a different outcome; the results still support the conclusion that 'compensatory growth' is active in shape regulation of the skull.

7.3.2 Sphenoid alternatives

In this calculation the sphenoid was substituted by different alternatives. The shape variances did not differ substantially between the sphenoid alternatives (Tab. 27 and Fig. 37). In the regression of the log-transformed shape variances on the log-transformed inverse bending energy the resulting regression slope was +0.85 for all sphenoid alternatives (Fig. 39). Therefore, the use of any of the alternatives did not result in a different outcome; the results still support the conclusion that 'compensatory growth' is active in shape regulation of the skull.

7.4 Shape calculation according to Bookstein (2015)

As mentioned in section 5, the sliding landmark algorithm reduces the variance of semilandmarks. Thus local deformations were visible in deformation grids of partial warps of such semilandmarks, reflecting the variance of their position along the curves (Fig. 40, 41 and 42). When only the last 21 partial warps were included in the calculation, the regression slope of the log-transformed shape variances regressed on the log-transformed inverse bending energy was +0.71, meaning that the indication for 'compensatory growth' was even more striking (Fig. 43).

Table 18: Alternative landmark assignments.

structure	assigned landmarks
sphenooccipital alternatives	
sphenooccipital	27, 29, 28, 39, 31, 34, 30
sphenooccipital excluding 27	29, 28, 39, 31, 34, 30
sphenooccipital excluding 28	27, 29, 39, 31, 34, 30
sphenooccipital excluding 27 and 28	29, 39, 31, 34, 30
sphenoid alternatives	
sphenoid	27, 29, 28, 39, 31, 34, 30
sphenoid excluding 27	29, 28, 39, 31, 34, 30
sphenoid excluding 28	27, 29, 39, 31, 34, 30
sphenoid excluding 27 and 28	29, 39, 31, 34, 30

Table 19: Area variances of the overall cranium with sphenooccipital for size analysis.

structure	area variance (in cm^2)
outline	1.90×10^4
sum of individual bones	1.07×10^4
frontal	335.30
parietal	214.95
occipitalpart	273.21
sphenooccipital	154.12
vomer	205.39
maxilla	60.09
nasal cavity	506.90
pseudonasal	21.69
braincase	8912.00

Table 20: Area variances divided by area means of the overall cranium with sphenooccipital for size analysis.

structure	area variance / area mean
outline	94.40
frontal	32.24
parietal	28.79
occipitalpart	33.30
sphenooccipital	17.12
vomer	34.81
maxilla	17.21
nasal cavity	35.15
pseudonasal	16.43
braincase	63.28
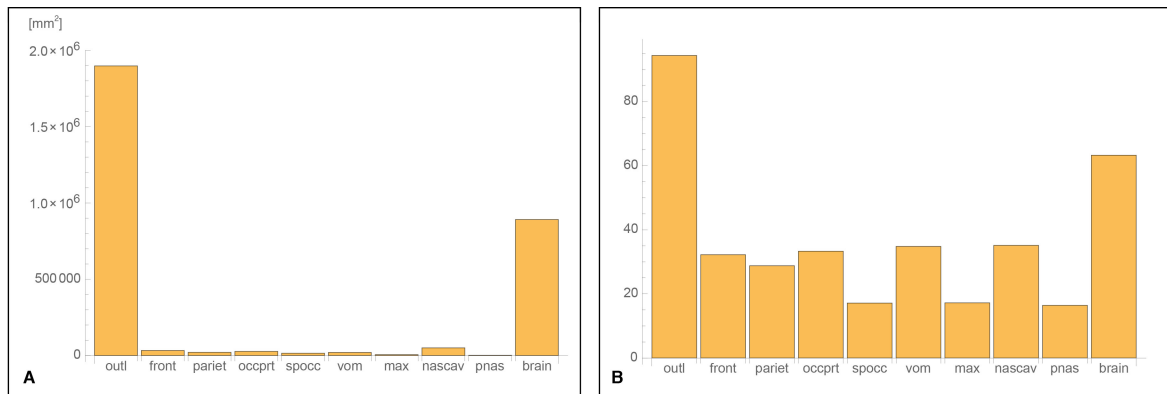
Figure 30: (A) Area variances of the overall cranium with sphenooccipital for size analysis. (B) Area variances divided by area means of the overall cranium with sphenooccipital for size analysis. Captions: outl = outline, front = frontal, pariet = parietal, occprt = occipitalpart, spocc = sphenooccipital, vom = vomer, max = maxilla, nascav = nasal cavity, pnas = pseudonasal, brain = braincase.

Table 21: Area variances for sphenooccipital alternatives for size analysis.

structure	area variance (in cm^2)
sphenooccipital	154.12
sphenooccipital excluding 27	140.71
sphenooccipital excluding 28	156.32
sphenooccipital excluding 27 and 28	140.88

Table 22: Area variances divided by area means for sphenooccipital alternatives for size analysis.

structure	area variance / area mean
sphenooccipital	17.12
sphenooccipital excluding 27	17.15
sphenooccipital excluding 28	19.58
sphenooccipital excluding 27 and 28	19.60
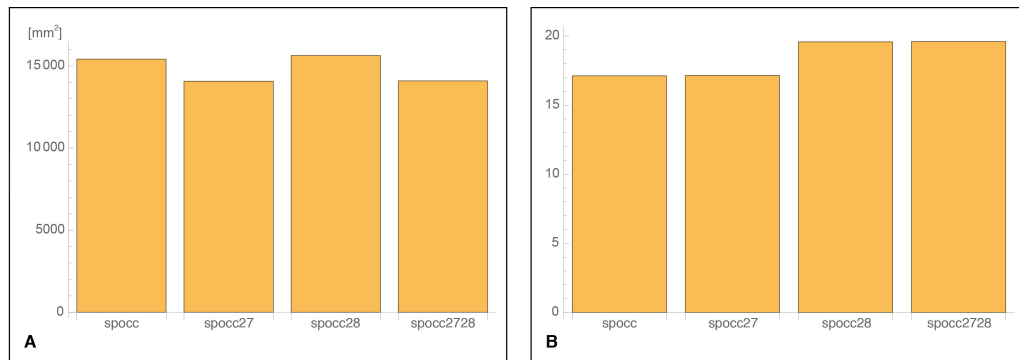
Figure 31: (A) Area variances for sphenooccipital alternatives for size analysis. (B) Area variances divided by area means for sphenooccipital alternatives for size analysis. Captions: spocc = sphenooccipital, spocc 27 = sphenooccipital excluding 27, spocc 28 = sphenooccipital excluding 28, spocc 2728 = sphenooccipital excluding 27 and 28.
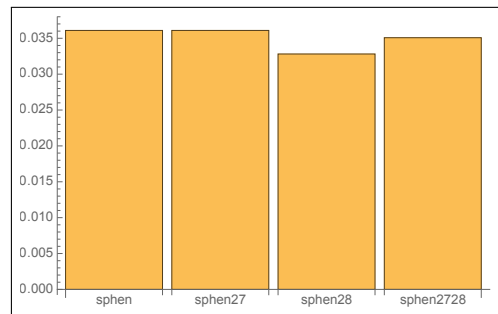
Table 23: Area variances for sphenoid alternatives for size analysis.

structure	area variance (in cm^2)
sphenoid	81.70
sphenoid excluding 27	77.14
sphenoid excluding 28	79.49
sphenoid excluding 27 and 28	73.66

Table 24: Area variances divided by area means for sphenoid alternatives for size analysis.

structure	area variance / area mean
sphenoid	14.65
sphenoid excluding 27	14.11
sphenoid excluding 28	17.44
sphenoid excluding 27 and 28	16.55
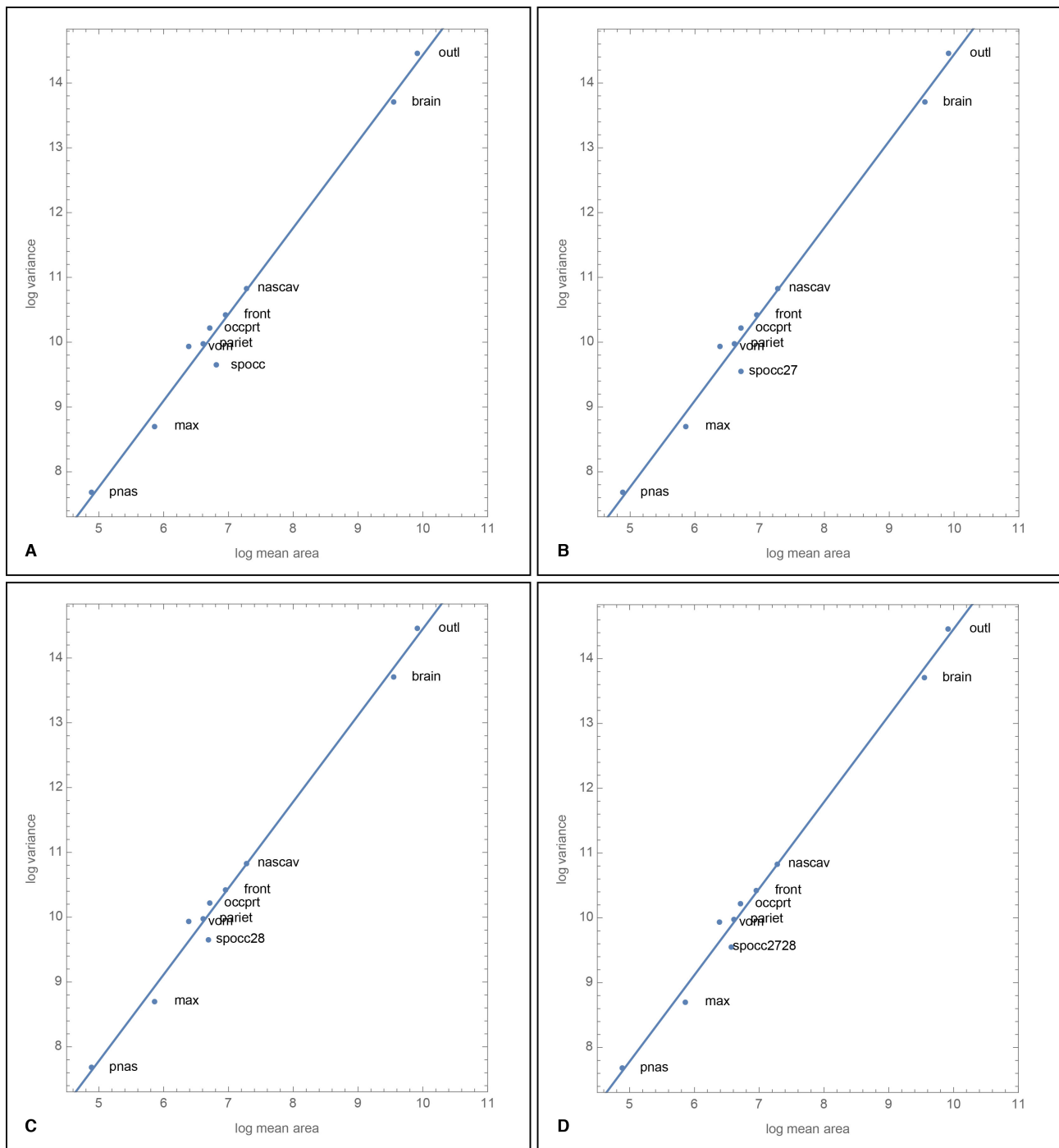
Figure 32: Log area variances regressed on log mean area with sphenooccipital alternatives for size analysis. (A) Log area variances regressed on log mean area with sphenooccipital. Regression slope = +1.33. (B) Log area variances regressed on log mean area with sphenooccipital excluding 27. Regression slope = +1.33. (C) Log area variances regressed on log mean area with sphenooccipital excluding 28. Regression slope = +1.33. (D) Log area variances regressed on log mean area with sphenooccipital excluding 27 and 28. Regression slope = +1.33.
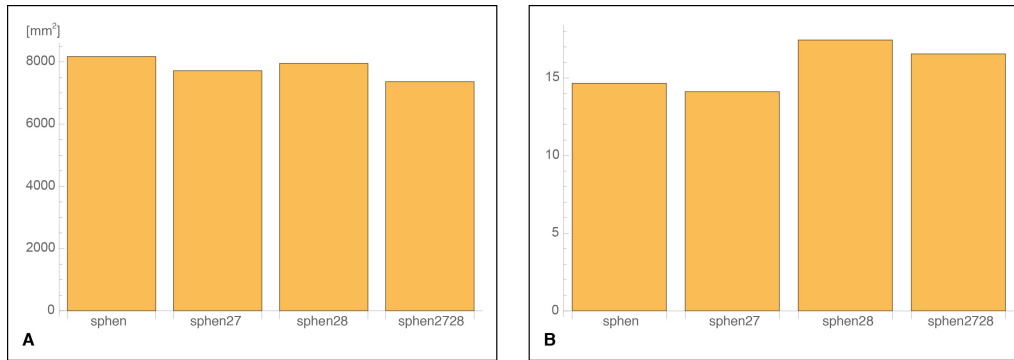
Figure 33: (A) Area variances for sphenoid alternatives for size analysis. (B) Area variances divided by area means for sphenoid alternatives for size analysis. Captions: sphen = sphenoid, sphen 27 = sphenoid excluding 27, sphen 28 = sphenoid excluding 28, sphen 2728 = sphenoid excluding 27 and 28.

Table 25: Shape variances for the overall cranium with sphenooccipital and occipitalpart.

structure	shape variance
outline	0.0054
frontal	0.0056
parietal	0.0032
occipitalpart	0.0120
sphenooccipital	0.0232
vomer	0.0312
ethmoid	0.0261
maxilla	0.0294
nasal cavity	0.0289
nasal	0.0072
braincase	0.0057

Table 26: Shape variances for sphenooccipital alternatives.

structure	shape variance
sphenooccipital	0.0232
sphenooccipital excluding 27	0.0200
sphenooccipital excluding 28	0.0224
sphenooccipital excluding 27 and 28	0.0191
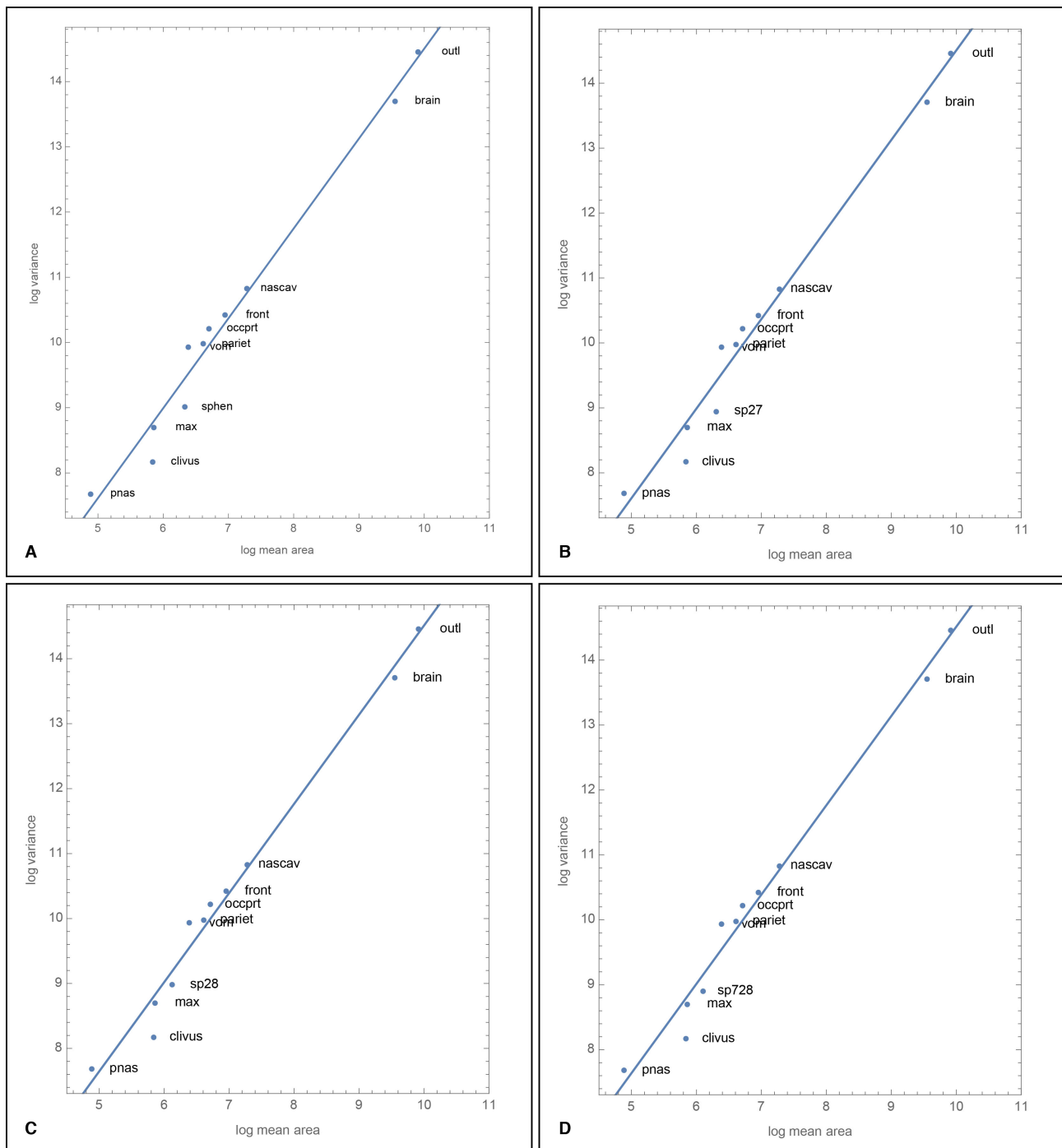
Figure 34: Log area variances regressed on log mean area with sphenoid and alternatives for size analysis. (A) Log area variances regressed on log mean area. Regression slope = +1.38. (B) Log area variances regressed on log mean area with sphenoid excluding 27. Regression slope = +1.38. (C) Log area variances regressed on log mean area with sphenoid excluding 28. Regression slope = +1.37. (D) Log area variances regressed on log mean area with sphenoid excluding 27 and 28. Regression slope = +1.37.
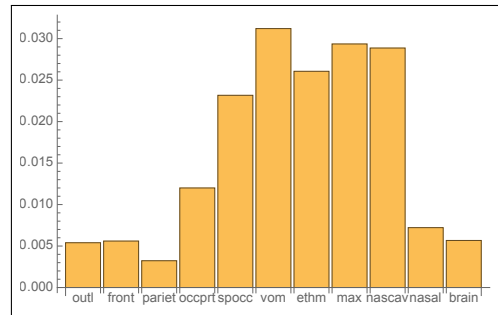
Figure 35: Shape variances for the overall cranium with sphenooccipital and occipitalpart.
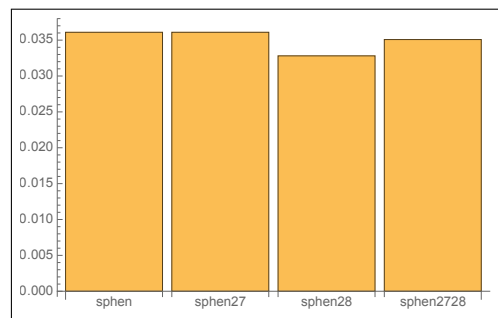
Figure 36: Shape variances for sphenooccipital alternatives. Captions: spocc = sphenooccipital, spocc 27 = sphenooccipital excluding 27, spocc 28 = sphenooccipital excluding 28, spocc 2728 = sphenooccipital excluding 27 and 28.

Figure 37: Shape variances for sphenoid alternatives. Captions: sphen = sphenoid, sphen 27 = sphenoid excluding 27, sphen 28 = sphenoid excluding 28, sphen 2728 = sphenoid excluding 27 and 28.

Table 27: Shape variances for sphenoid alternatives.

structure	shape variance
sphenoid	0.0361
sphenoid excluding 27	0.0361
sphenoid excluding 28	0.0328
sphenoid excluding 27 and 28	0.0350
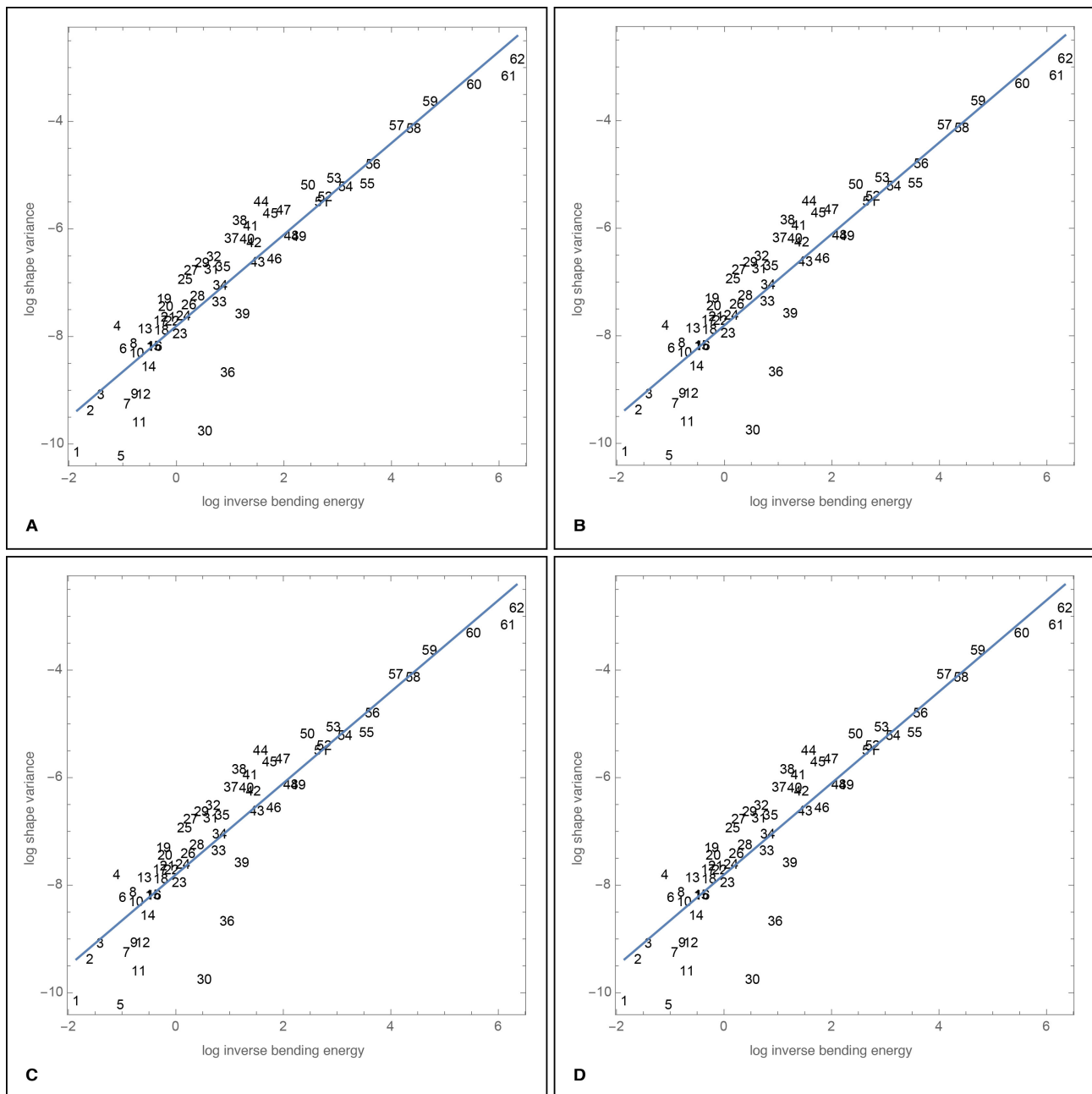
Figure 38: Log shape variances regressed on log inverse bending energy with sphenooccipital or alternatives and occipitalpart. (A) Log shape variances regressed on log inverse bending energy with sphenooccipital and occipitalpart. Regression slope = +0.85. (B) Log shape variances regressed on log inverse bending energy with sphenooccipital excluding 27 and occipitalpart. Regression slope = +0.85. (C) Log shape variances regressed on log inverse bending energy with sphenooccipital excluding 28 and occipitalpart. Regression slope = +0.85. (D) Log shape variances regressed on log inverse bending energy with sphenooccipital excluding 27 and 28 and occipitalpart. Regression slope = +0.85.
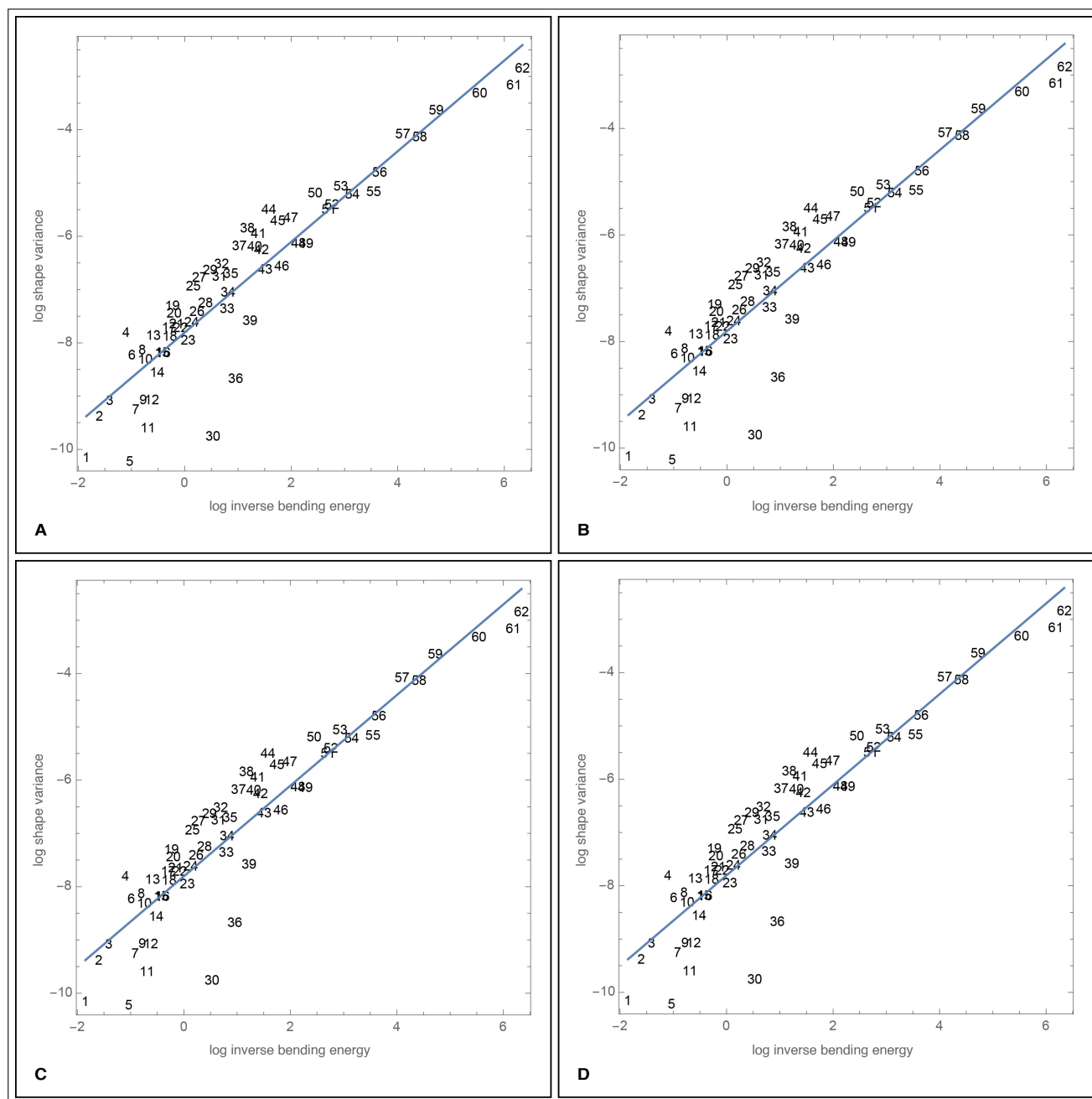
Figure 39: Log shape variances regressed on log inverse bending energy with sphenoid or alternatives and occipitalpart. (A) Log shape variances regressed on log inverse bending energy. Regression slope = +0.85. (B) Log shape variances regressed on log inverse bending energy with sphenoid excluding 27 and occipitalpart. Regression slope = +0.85. (C) Log shape variances regressed on log inverse bending energy with sphenoid excluding 28 and occipitalpart. Regression slope = +0.85. (D) Log shape variances regressed on log inverse bending energy with sphenoid excluding 27 and 28 and occipitalpart. Regression slope = +0.85.
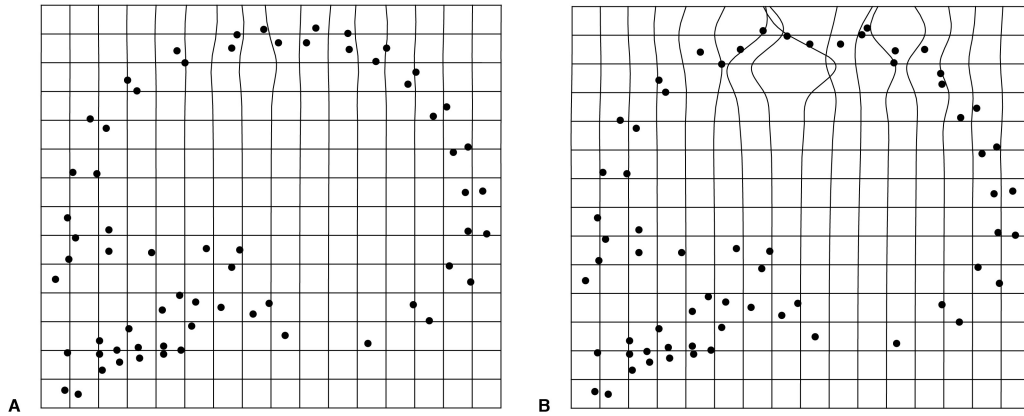
Figure 40: (A) Local deformation for partialwarp of semilandmark No. 5. (B) Extrapolated local deformation for partialwarp of semilandmark No. 5.
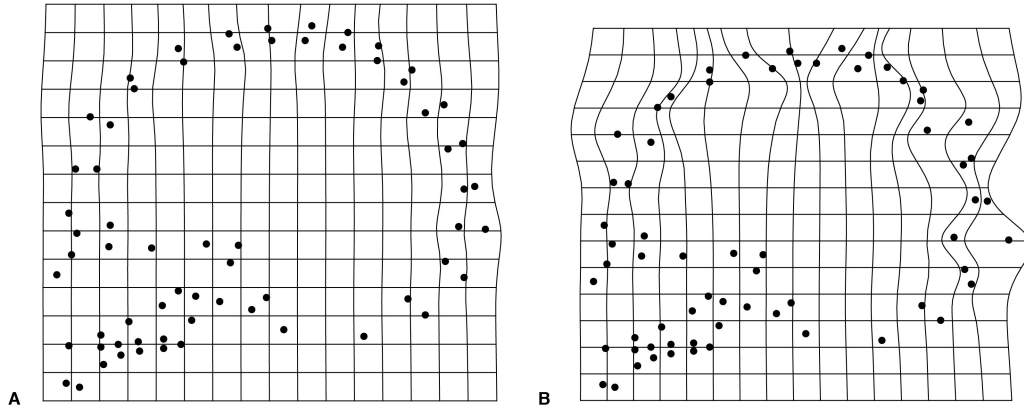
Figure 41: (A) Local deformation for partialwarp of semilandmark No. 14. (B) Extrapolated local deformation for partialwarp of semilandmark No. 14.
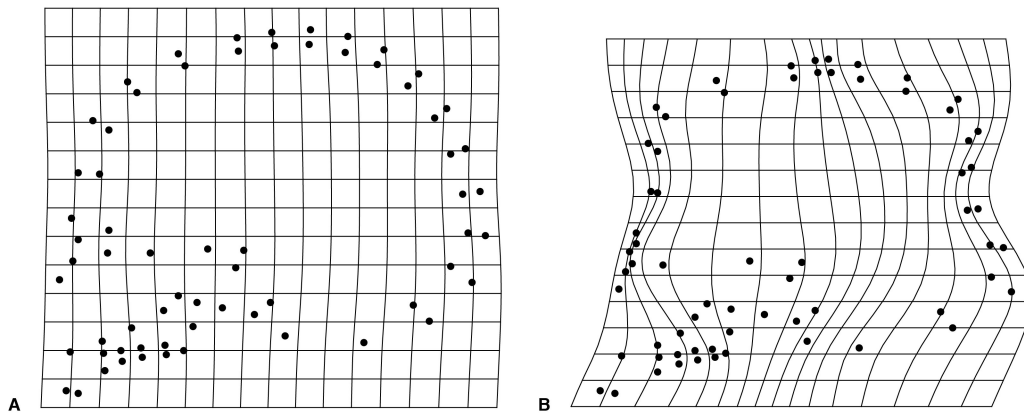
Figure 42: (A) Local deformation for partialwarp of semilandmark No. 52. (B) Extrapolated local deformation for partialwarp of semilandmark No. 52.
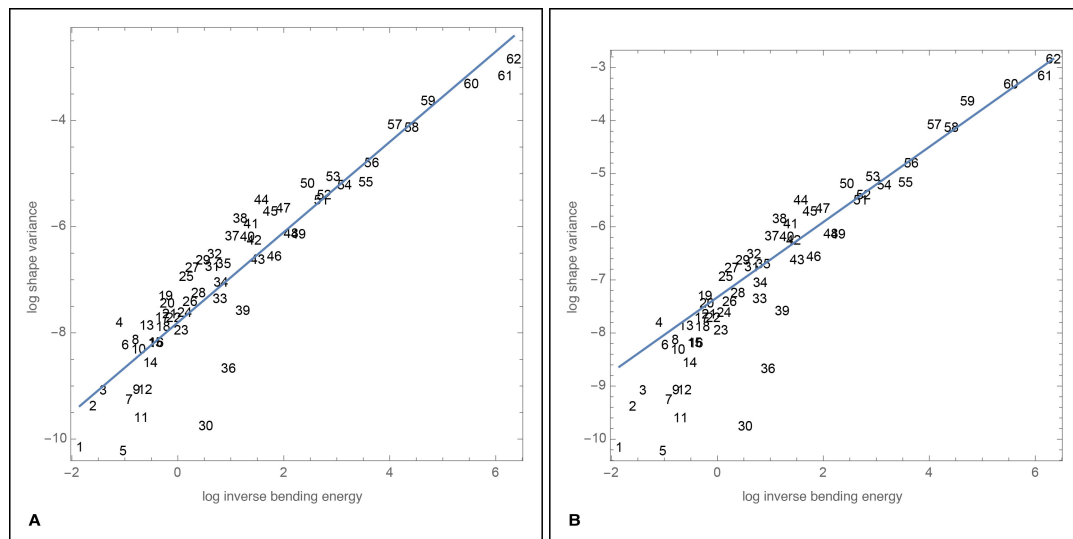
Figure 43: (A) Log shape variances regressed on log inverse bending energy for all partial warps. Regression slope = +0.85. (B) Log shape variances regressed on log inverse bending energy for partial warps 42 to 62. Regression slope = +0.71.

References

Ackermann, R. R. (2002). "Patterns of covariation in the hominoid craniofacial skeleton: implications for paleoanthropological models." In: *J. Hum. Evol.* 43, pp. 167–187.

Ankel-Simons, F. (2007). *Primate Anatomy. An Introduction.* Elsevier Academic Press.

Berg, R. L. (1960). "The ecological significance of correlation pleiades." In: *Evolution* 14, pp. 171–180.

Bookstein, F. L. (1997). "Landmark methods for forms without landmarks: morphometrics of group differences in outline shape". In: *Med. Image Anal* 1.3, pp. 225–243.

Bookstein, F. L. (2015). "Integration, Disintegration, and Self-Similarity: Characterizing the Scales of Shape Variation in Landmark Data". In: *Evolutionary Biology*, pp. 1–32. ISSN: 0071-3260. DOI: `10.1007/s11692-015-9317-8`.

Burger, E. H. and J Klein-Nulend (1999). "Mechanotransduction in bone–role of the lacuno-canalicular network." In: *The FASEB journal* 13.Supplement, S101–S112. ISSN: 0892-6638.

Chambers, T. J. (1991). "Regulation of Osteoclastic Bone Reorption In Vitro". In: *Bone. Volume 2. The Osteoclast.* Ed. by B. K. Hall. CRC Press, pp. 141–173.

Cheverud, J. M. (1982). "Phenotypic, genetic, and environmental morphological integration in the cranium." In: *Evolution* 36, pp. 499–516.

Cheverud, J. M. (1996a). "Developmental integration and the evolution of pleiotropy." In: *American Zoologist* 36, pp. 44–50.

Cheverud, J. M. (1996b). "Quantitative genetic analysis of cranial morphology in the cotton-top (Saguinus oedipus) and saddle-back (S. fuscicollis) tamarins." In: *Journal of Evolutionary Biology* 9, pp. 5–42.

Drake, A. G. and C. P. Klingenberg (2010). "Large-scale diversification of skull shape in domestic dogs: disparity and modularity." In: *Am. Nat.* 175, pp. 289–301.

Dryden, I. L. and K. V. Mardia (1998). *Statistical Shape Analysis.* New York: John Wiley & Sons.

Frost, H. M. (1987). "Bone "mass" and the "mechanostat". A proposal." In: *Anatomical Record* 219, pp. 1–9.

Frost, H. M. (1998). "From Wolff's law to the mechanostat: A new 'face' of physiology". In: *Journal of Orthopaedic Science* 3.5, pp. 282–286. ISSN: 09492658. DOI: `10.1007/s007760050054`.

Frost, H. M. (2003). "Bone's mechanostat: a 2003 update." In: *The Anatomical Record Part A* 275A, pp. 1081–1101. ISSN: 1552-4884. DOI: `10.1002/ar.a.10119`.

Gerard, R. W., ed. (1958). *Concepts of Biology.* National Academy of Sciences, p. 140.

Goswami, A (2006). "Morphological integration in the carnivoran skull." In: *Evolution* 60, pp. 169–183.

Gower, J (1975). "Generalized procrustes analysis". In: *Psychometrika* 40.1, pp. 33–51.

Gunz, P. and P. Mitteroecker (2013). "Semilandmarks: a method for quantifying curves and surfaces". In: *Hystrix* 24.1.

Gunz, P., P. Mitteroecker, and F. L. Bookstein (2005). "Semilandmarks in Three Dimensions". In: *Modern Morphometrics in Physical Anthropology*. Ed. by D. E. Slice. New York: Kluwer Press, pp. 73–98.

Hall, B. K. (2015). *Bones and Cartilage*. Elsevier. ISBN: 9780124166783. DOI: `10.1016/B978-0-12-416678-3.00048-3`.

Hallgrímsson, B. (1999). "Ontogenetic Patterning of Skeletal Fluctuating Asymmetry in Rhesus Macaques and Humans: Evolutionary and Developmental Implications". In: *International Journal of Primatology* 20.1, pp. 121–151. DOI: `10.1023/A:1020540418554`.

Hallgrímsson, B., J. J. Y. Brown, A. F. Ford-Hutchinson, H. D. Sheets, M. L. Zelditch, and F. R. Jirik (2006). "The brachymorph mouse and the developmental-genetic basis for canalization and morphological integration". In: *Evolution and Development* 8.1, pp. 61–73. ISSN: 1520541X. DOI: `10.1111/j.1525-142X.2006.05075.x`.

Hallgrimsson, B., D. E. Lieberman, N. M. Young, T. Parsons, and S. Wat (2007). "Evolution of covariance in the mammalian skull". In: *Novartis Foundation Symposium* 284, 164–185; discussion 185–190. ISSN: 1528-2511.

Hallgrímsson, B., H. Jamniczky, N. M. Young, C. Rolian, E Trish, J. C. Boughner, and R. S. Marcucio (2009). *Deciphering the Palimpsest: Studying the Relationship Between Morphological Integration and Phenotypic Covariation*. Vol. 36. 4, pp. 355–376. ISBN: 1169200990. DOI: `10.1007/s11692-009-9076-5.Deciphering`.

Hansen, T. F. and D. Houle (2008). "Measuring and comparing evolvability and constraint in multivariate characters". In: *Journal of Evolutionary Biology* 21, pp. 1201–1219. ISSN: 1010061X. DOI: `10.1111/j.1420-9101.2008.01573.x`.

Hansen, T. F. (2003). "Is modularity necessary for evolvability? Remarks on the relationship between pleiotropy and evolvability". In: *BioSystems* 69, pp. 83–94. ISSN: 03032647. DOI: `10.1016/S0303-2647(02)00132-6`.

Huiskes, R, R Ruimerman, G. H. van Lenthe, and J. D. Janssen (2000). "Effects of mechanical forces on maintenance and adaptation of form in trabecular bone." In: *Nature* 405, pp. 704–706.

Jaalouk, D. E. and J. Lammerding (2009). "Mechanotransduction gone awry." In: *Nature reviews. Molecular cell biology* 10, pp. 63–73. ISSN: 1471-0072. DOI: `10.1038/nrm2597`.

Jiang, X., S. Iseki, R. E. Maxson, H. M. Sucov, and G. M. Morriss-Kay (2002). "Tissue origins and interactions in the mammalian skull vault." In: *Developmental biology* 241.1, pp. 106–16. ISSN: 0012-1606. DOI: `10.1006/dbio.2001.0487`.

Junqueira, L. C. U. and J. Carneiro (2005). *Histologie.* Ed. by M. Gratzl. Springer Medizin Verlag.

Kahn, A. J. and N. C. Partridge (1991). "Bone Resorption In Vivo". In: *Bone. Volume 2. The Osteo-clast.* Ed. by B. K. Hall. CRC Press, pp. 119–140.

Kellner, J. R. and R. A. Alford (2003). "The ontogeny of fluctuating asymmetry." In: *The American Naturalist* 161.6, pp. 931–947. ISSN: 0003-0147. DOI: 10.1086/375177.

Lieberman, D. E., B McBratney, and G Krowitz (2002). "The evolution and development of cranial form in Homo sapiens." In: *Proc. Natl. Acad. Sci. USA* 99, pp. 1134–1139.

Marcucio, R. S., D. R. Cordero, D. Hu, and J. A. Helms (2005). "Molecular interactions coordinating the development of the forebrain and face." In: *Developmental biology* 284.1, pp. 48–61. ISSN: 0012-1606. DOI: 10.1016/j.ydbio.2005.04.030.

Marroig, G, L. T. Shirai, A Porto, F. B. de Oliveira, and V De Conto (2009). "The evolution of modularity in the mammalian skull II: evolutionary consequences." In: *Evol. Biol.* 36, pp. 136–148.

Martin, R and K Saller (1957). *Lehrbuch der Anthropologie.* Gustav Fischer, Stuttgart, pp. 488–490.

Mays, S. (1998). *The Archaeology of Human Bones.* Routledge.

Meulen, M. C. H. van der and R. Huiskes (2002). "Why mechanobiology? A survey article." In: *Journal of Biomechanics* 35.4, pp. 401–14. ISSN: 0021-9290.

Mitteroecker, P. (2009). "The Developmental Basis of Variational Modularity: Insights from Quantitative Genetics, Morphometrics, and Developmental Biology". In: *Evolutionary Biology* 36, pp. 377–385.

Mitteroecker, P. and F. Bookstein (2008). "The evolutionary role of modularity and integration in the hominoid cranium". In: *Evolution* 62.4, pp. 943–958.

Mitteroecker, P., P. Gunz, S. Neubauer, and G. Müller (2012). "How to Explore Morphological Integration in Human Evolution and Development?" In: *Evolutionary Biology* 39.4, pp. 536–553. ISSN: 00713260. DOI: 10.1007/s11692-012-9178-3.

Mitteroecker, P., P. Gunz, S. Windhager, and K. Schaefer (2013). "A brief review of shape, form, and allometry in geometric morphometrics, with applications to human facial morphology". In: *Hystrix* 42.1, pp. 59–66.

Müller, G. B. (2007). "Evo-devo: extending the evolutionary synthesis". In: *Nature reviews. Genetics* 8.12, pp. 943–949. ISSN: 1471-0056. DOI: 10.1038/nrg2219.

Nowlan, N. C., P. Murphy, and P. J. Prendergast (2008). "A dynamic pattern of mechanical stimulation promotes ossification in avian embryonic long bones." In: *Journal of Biomechanics* 41.2, pp. 249–58. ISSN: 0021-9290. DOI: 10.1016/j.jbiomech.2007.09.031.

Olson, E. C. and R. L. Miller (1958). *Morphological Integration.* Chicago: University of Chicago Press.

Opperman, L. A. (2000). "Cranial Sutures as Intramembranous Bone Growth Sites". In: *Developmental Dynamics* 219.4, pp. 472–485. ISSN: 1058-8388.

Pavlicev, M. and T. F. Hansen (2011). "Genotype-Phenotype Maps Maximizing Evolvability: Modularity Revisited". In: *Evolutionary Biology* 38, pp. 371–389. ISSN: 00713260. DOI: 10.1007/s11692-011-9136-5.

Porto, A., F. B. de Oliveira, L. T. Shirai, V. De Conto, and G. Marroig (2009). "The evolution of modularity in the mammalian skull I: morphological integration patterns and magnitudes". In: *Evol Biol* 36, pp. 118–135.

Putz, R and R Pabst, eds. (2008). *Sobotta - Anatomie des Menschen*. Elsevier.

Rohlf, F. J. and D. E. Slice (1990). "Extensions of the Procrustes method for the optimal superimposition of landmarks". In: *Systematic Zoology* 39, pp. 40–59.

Roseman, C. C., T. D. Weaver, and C. B. Stringer (2011). "Do modern humans and Neandertals have different patterns of cranial integration?" In: *Journal of Human Evolution* 60, pp. 684–693.

Ruimerman, R. and R. Huiskes (2005). *Development of a unifying theory for mechanical adaptation and maintenance of trabecular bone*.

Schmalhausen, I. I. (1949). *Factors of Evolution*. University of Chicago Press.

Singh, N., K. Harvati, J.-J. Hublin, and C. P. Klingenberg (2012). "Morphological evolution through integration: A quantitative study of cranial integration in Homo, Pan, Gorilla and Pongo". In: *Journal of Human Evolution* 62, pp. 155–164.

Skerry, T. (2000). "Biomechanical influences on skeletal growth and development". In: *Development, Growth and Evolution. Implications for the Study of the Hominid Skeleton*. Ed. by P O'Higgins and M. Cohn. Academic Press, pp. 29–55.

Skerry, T. M. and L. J. Suva (2003). "Investigation of the regulation of bone mass by mechanical loading: From quantitative cytochemistry to gene array". In: *Cell Biochemistry and Function* 21, pp. 223–229. ISSN: 02636484. DOI: 10.1002/cbf.1077.

Spector, J. A., J. A. Greenwald, S. M. Warren, P. J. Bouletreau, R. C. Detch, P. J. Fagenholz, F. E. Crisera, and M. T. Longaker (2002). "Dura mater biology: autocrine and paracrine effects of fibroblast growth factor 2". In: *Plastic and reconstructive surgery* 109.2, pp. 645–654. ISSN: 0032-1052. DOI: 10.1097/00006534-200202000-00035.

Stearns, S. C., M. Kaiser, and T. J. Kawecki (1995). "The differential genetic and environmental canalization of fitness components in Drosophila melanogaster". In: *Journal of Evolutionary Biology* 8.5, pp. 539–557.

Terentjev, P. V. (1931). "Biometrische Untersuchungen über die morphologischen Merkmale von Rana ridibunda Pall." In: *Biometrika* 23, pp. 23–51.

Teschler-Nicola, M. and P. Mitteroecker (2007). "Von künstlicher Kopfformung". In: *Attila und die Hunnen*. Stuttgart: Konrad Theiss Verlag GmbH, pp. 271–281. ISBN: 978-3-930239-18-4.

Waddington, C. H. (1942). "Canalization of development and the inheritance of aqcuired characters". In: *Nature* 150, pp. 563–565.

Wagner, G. P. and L. Altenberg (1996). "Complex adaptations and the evolution of evolvability". In: *Evolution* 50.3, pp. 967–976.

Wagner, G. P., G. Booth, and H. Bagheri-Chaichian (1997). "A Population Genetic Theory of Canalization". In: *Evolution* 51.2, pp. 329–347.

White, T. D. and P. A. Folkens (1991). *Human Osteology*. San Diego: Elsevier Academic Press.

White, T. D. and P. A. Folkens (2005). *The Human Bone Manual*. Amsterdam: Elsevier Academic Press.

Willmore, K. E., L. Leamy, and B. Hallgrímsson (2006). "Effects of developmental and functional interactions on mouse cranial variability through late ontogeny". In: *Evolution and Development* 8.6, pp. 550–567. ISSN: 1520541X. DOI: 10.1111/j.1525-142X.2006.00127.x.

Wolff, J. (1892). *Das Gesetz der Transformation der Knochen*. Berlin: A. Hirschwald.

Yu, J. C., J. H. Lucas, K. Fryberg, and J. L. Borke (2001). "Extrinsic Tension Results in FGF-2 Release, Membrane Permeability Change, and Intracellular Ca ++ Increase in Immature Cranial Sutures". In: *Journal of Craniofacial Surgery* 12.4. ISSN: 1049-2275.

Zelditch, M. L. and A. C. Carmichael (1989). "Ontogenetic variation in patterns of developmental and functional integration in skulls of Sigmodon fulviventer." In: *Evolution* 43, pp. 814–824.

Zelditch, M. L., B. L. Lundrigan, and T. Garland Jr. (2004). "Developmental regulation of skull morphology. I. Ontogenetic dynamics of variance". In: *Evolution & Development* 206, pp. 194–206.

Zelditch, M. L., J. Mezey, D. H. Sheets, B. L. Lundrigan, and T. Garland Jr. (2006). "Developmental regulation of skull morphology II: ntogenetic dynamics of covariance". In: *Evolution & Development* 60, pp. 46–60.

List of Figures

List of Tables

8   Acknowledgements

I would like to thank some people who were directly or indirectly involved in writing this thesis. First of all, my supervisor Ass.-Prof. Mag. Dr. Philipp Mitteröcker, who gave me the opportunity to work on this project and who devised the model this thesis has worked with. I thank him for his helpful and patient feedback and supervision as well as for the education in statistics and morphometrics I have received from him. Furthermore, I would like to thank DDr. Fred Bookstein for helpful input and discussion on the approach of this thesis. I also thank all colleagues at the Department of Theoretical Biology at the University of Vienna for their feedback and comments on my work. Many thanks also to my colleague Tim Peterson, who helpfully directed me towards mechanotransductive pathways.

Further thanks go to my family, who have emotionally supported me and provided me with kind words when necessary throughout the course of my studies. I would especially like to thank my fiancé, Dipl.-Ing. Christoph Erkinger, without whom I would have navigated work, my studies and writing this thesis much less successfully. I thank him for his support.

9   Curriculum Vitae

Personal information

Name	Corinna Matiasch, BSc
Address	Ettenreichgasse 48/2/22, 1100 Vienna
University address	Department of Theoretical Biology, University Vienna
	Althanstraße 14, 1090 Vienna
Phone	(+43) 664 518 48 42
E-Mail	corinna.matiasch@gmail.com
Born	February 25th, 1988 in Vienna
Nationality	Austria

Education

since Oct. 2012	Teacher Training Program for Biology and Environmental Studies & English at the University of Vienna
since Oct. 2011	Master's degree program Anthropology at the University of Vienna
Oct. 2011	BSc thesis "Makroskopische Diagnosen und metrische Analysen an einem menschlichen Individuum aus dem awarenzeitlichen Gräberfeld Wien-Csokorgasse"
March 2008–Oct. 2011	Bachelor's degree program Biology
	Oct. 2009 start of specialization in Anthropology
Oct. 2006–Feb. 2007	Medicine Degree Program at the Medical University of Vienna
1998–2006	AHS Rainergasse, BrG 5, Vienna (grammar school)
	June 2006 graduation with Matura
1994–1996	Volksschule Pannaschgasse, 1050 Vienna (elementary school)

Job Experience

since Jan. 2008	John Harris Fitness - Uniqa Vital Center, receptionist
	Nov. 2008: promotion to Vice Front Desk Manager
	Dec. 2014: promotion to Front Desk Manager
March 2007–June 2008	Billa, cashier
Sept 2006–March 2007	Ströck Bäckerei, vendor

JULY 2006–SEPT. 2006	Service Center Rotes Kreuz Blutspendezentrale, telephonist
OCT. 2003–JULY 2006	St. Florian, tutor
JULY 2004	Wiener Städtische Versicherungen AG, office worker

PRACTICAL EXPERIENCE

APRIL 2010–FEB. 2012	Natural History Museum Vienna, volunteer in the Department of Anthropology
	celtic settlement Roseldorf – cleaning of skeletal remains from the latène period
	cemetery Pottenbrunn – diagnosis of pathological leprous changes in skeletal remains from the early middle ages

EDITING EXPERIENCE

Anabolic-androgenic steroid abuse: Blood cell count, lipid profile, liver function, hormones and symptoms in a doping-free period – J. Ott, R. Promberger, J.C. Huber, P. Frigo (submitted to European Journal of Applied Physiology)

Venous thrombembolism, thrombophilic defects, combined oral contraception and anticoagulation – J. Ott, R. Promberger, U. Kaufmann, J. Huber, P. Frigo (Archives of Gynecology and Obstetrics. 2009 Nov; 280(5):811-4)

Dinner Cancelling and its effect on nocturnal Growth-Hormone Kinetics – P. Frigo, J. Ott, K. Renezeder, W. Eppel, J.C. Huber (Geburtshilfe und Frauenheilkunde. 2008; 68(1):2-14)

Laparoscopic ovarian tissue harvesting for cryopreservation – an effective and safe procedure for fertility preservation – K. Mayerhofer, J. Ott, K. Nouri, L. Stögbauer, E.M. Fischer, M. Lipovac, J.C. Huber (European Journal of Obstetrics, Gynecology and Reproductive Bioliology. 2010 Sep; 152(1):68-72)

Quality of Life and Treatment Satisfaction of Transsexuals – S. Aust, U. Kaufmann, J. Ott (Geburtshilfe und Frauenheilkunde. 2011; 71(5):314)

Villous Mucinous Cystadenoma of the Appendix in a Postmenopausal Woman – K. Nouri, M. Demmel, J. Ott, R. Promberger, J.C. Huber, K. Mayerhofer (Journal of the Society of Laproendoscopic Surgeons. 2010 Apr-Jun; 14(2): 296–298)

Skills

German	native language
English	fluent
	FCE – First Certificate of English (Level B2)
	CAE – Certificate of Advanced English (Level C1)
French	basic knowledge
	D.E.L.F. 1 – Diplôme d'Ètudes en Langue Française, 1er degré
Latin	4 years in school
IT	Windows, Microsoft Office
	Mac OS, iWork
	Open Office
	Adobe Suite: Photoshop, Illustrator, Acrobat Reader
	Wolfram Mathematica
	Amira
	LaTeX